

Distribution Agreement

In presenting this thesis as a partial fulfillment of the requirements for a degree from Emory University, I hereby grant to Emory University and its agents the non-exclusive license to archive, make accessible, and display my thesis in whole or in part in all forms of media, now or hereafter known, including display on the World Wide Web. I understand that I may select some access restrictions as part of the online submission of this thesis. I retain all ownership rights to the copyright of the thesis. I also retain the right to use in future works (such as articles or books) all or part of this thesis.

Aaron Wozniak

April 10, 2023

Liver GALT Restoration Mediated by AAV8 Gene Therapy

by

Aaron Wozniak

Dr. Judith Fridovich-Keil

Adviser

Chemistry

Dr. Judith Fridovich-Keil

Adviser

Dr. David Lynn

Committee Member

Dr. Richard Himes

Committee Member

2023

Liver GALT Restoration Mediated by AAV8 Gene Therapy

by

Aaron Wozniak

Dr. Judith Fridovich-Keil

Adviser

An abstract of
a thesis submitted to the Faculty of Emory College of Arts and Sciences
of Emory University in partial fulfillment
of the requirements of the degree of
Bachelor of Science with Honors

Chemistry

2023

Abstract

Liver GALT Restoration Mediated by AAV8 Gene Therapy by Aaron Wozniak

Classic galactosemia is a genetic disorder characterized by a deficiency of functional galactose 1-phosphate uridylyl transferase (GALT). The GALT enzyme catalyzes a critical reversible reaction within the Leloir pathway of galactose metabolism where galactose 1-phosphate (gal-1P) is reversibly converted into UDP-galactose. Failure to produce adequate levels of functional GALT results in the accumulation of multiple metabolites associated with the Leloir pathway in tissues throughout the body. This study aims to discern if liver specific GALT restoration can be achieved through the use of AAV8 gene therapy in a GALT-null rat model of CG. GALT activity was assessed using GALT assays in liver and brain tissues to determine if the transgene was expressed within these tissues. Enzyme assays were performed on tissues collected from rats at 14, 30, 45, and 60 days after the administration of treatment to measure the amount and duration of GALT activity in treated animals. The results of the assays showed GALT activity in the livers of treated GALT-null rats, while brain GALT activity remained below detectable limits. After GALT activity was detected in the livers of treated animals, galactose, galactitol, and gal-1P metabolite levels were quantified in liver and brain tissue, while galactose and galactitol levels were measured in plasma samples. Metabolite levels were examined to determine if liver specific GALT restoration could provide meaningful decreases to liver metabolite levels in addition to those of the brain and plasma. Results indicated that there may be a pattern of decreased metabolite accumulation within all tissues analyzed. Overall, this experiment demonstrates liver specific GALT restoration can be achieved using an AAV8 virus. In addition, metabolite data suggest liver GALT activity may provide some correction to metabolite levels in the liver as well as other tissues and blood components throughout the organism.

Liver GALT Restoration Mediated by AAV8 Gene Therapy

by

Aaron Wozniak

Dr. Judith Fridovich-Keil

Adviser

A thesis submitted to the Faculty of Emory College of Arts and Sciences
of Emory University in partial fulfillment
of the requirements of the degree of
Bachelor of Science with Honors

Chemistry

2023

Acknowledgements

I would like to thank the other members of the Fridovich-Keil lab for their encouragement throughout this process. Special thanks to my adviser, Dr. Judith Fridovich-Keil for providing continuous guidance during this project and throughout my time as an undergraduate. I would also like to thank Dr. Shauna Rasmussen for performing all tail-vein injections, the vast majority of perfusions, and general rat colony maintenance, while also supporting me both inside and outside of the lab. This thesis would not have been possible without her work. I am also grateful for the help of Emory Wilson in collecting the liver and brain metabolite data. Additionally, I would like to thank my committee members Dr. David Lynn and Dr. Richard Himes. Lastly, I would like to express my deepest gratitude to Sneh Patel for his assistance and friendship during my time at the Fridovich-Keil lab, and Lingyuan Wu for teaching me the enzyme assay protocol and keeping the HPLC machines in working order.

Table of Contents

Chapter 1: Background	1
Chapter 2: Liver GALT Restoration by AAV8-Gene Therapy in GALT-null Rats	9
Chapter 3: Metabolic Efficacy of Liver GALT Restoration by AAV8-Mediated Gene Therapy in GALT-null Rats	27
Chapter 4: General Discussion	56
References	61

Tables

Table 1: Demographic Information of GALT Enzyme Assay Samples	10
Table 2: Final Dilutions Used in GALT Enzyme Assay	12
Table 3: PA10 Column Enzyme Assay Buffer Gradient Cycle	14
Table 4: PA10 Column Metabolite Buffer Gradient Cycle	30
Table 5: MA1 Column Metabolite Buffer Gradient Cycle	30

Figures

Figure 1: The Leloir Pathway of galactose metabolism 2

Figure 2: Liver GALT activity 15

Figure 3: 14 days post-injection liver GALT activity 16

Figure 4: 30 days post-injection liver GALT activity 17

Figure 5: 45 days post-injection liver GALT activity 18

Figure 6: 60 days post-injection liver GALT activity 19

Figure 7: Brain GALT activity 20

Figure 8: 14 days post-injection brain GALT activity 21

Figure 9: 30 days post-injection brain GALT activity 22

Figure 10: 45 days post-injection brain GALT activity 23

Figure 11: 60 days post-injection brain GALT activity 24

Figure 12: Liver galactose levels 32

Figure 13: Liver galactitol levels 33

Figure 14: Liver galactose 1-phosphate levels 34

Figure 15: 14 days post-injection liver galactose and galactitol levels 35

Figure 16: 30 days post-injection liver galactose and galactitol levels	35
Figure 17: 45 days post-injection liver galactose and galactitol levels	36
Figure 18: 60 days post-injection liver galactose and galactitol levels	36
Figure 19: Brain galactose levels	38
Figure 20: Brain galactitol levels	39
Figure 21: Brain galactose 1-phosphate levels	40
Figure 22: 14 days post-injection brain galactose and galactitol levels	41
Figure 23: 30 days post-injection brain galactose and galactitol levels	41
Figure 24: 45 days post-injection brain galactose and galactitol levels	42
Figure 25: 60 days post-injection brain galactose and galactitol levels	43
Figure 26: Plasma galactose levels	44
Figure 27: Plasma galactitol levels	45
Figure 28: 14 days post-injection plasma galactose and galactitol levels	46
Figure 29: 30 days post-injection plasma galactose and galactitol levels	46
Figure 30: 45 days post-injection plasma galactose and galactitol levels	47
Figure 31: 60 days post-injection plasma galactose and galactitol levels	47

Figure 32: Relationship between liver galactose and liver GALT activity	49
Figure 33: Relationship between liver galactitol and liver GALT activity	50
Figure 34: Relationship between liver galactose 1-phosphate and liver GALT activity	50
Figure 35: Relationship between brain galactose and liver GALT activity	51
Figure 36: Relationship between brain galactitol and liver GALT activity	51
Figure 37: Relationship between brain galactose 1-phosphate and liver GALT activity	52
Figure 38: Relationship between plasma galactose and liver GALT activity	52
Figure 39: Relationship between plasma galactitol and liver GALT activity	53

CHAPTER 1 BACKGROUND

Classic Galactosemia

Classic galactosemia (CG) is an autosomal recessive disorder stemming from a deficiency in functional galactose-1-phosphate uridylyl transferase (GALT) (1). This enzyme catalyzes the reversible transfer of an UMP-moiety from UDP-glucose first to a histidine in the active site of the enzyme, and then to galactose 1-phosphate (Gal-1P), forming UDP-galactose (UDPgal) (2). Failure to produce adequate functional GALT blocks the metabolism of galactose by the Leloir Pathway (Figure 1), resulting in the accumulation of galactose and Gal-1P. As galactose accumulates to abnormally high levels, it also becomes a substrate for aldose reductase and galactose dehydrogenase, that convert it into galactitol and galactonate, respectively (3). CG is inherited through pathogenic *GALT* alleles; one of the most common genotypes among patients of Northern European ancestry being Q188R/Q188R (4).

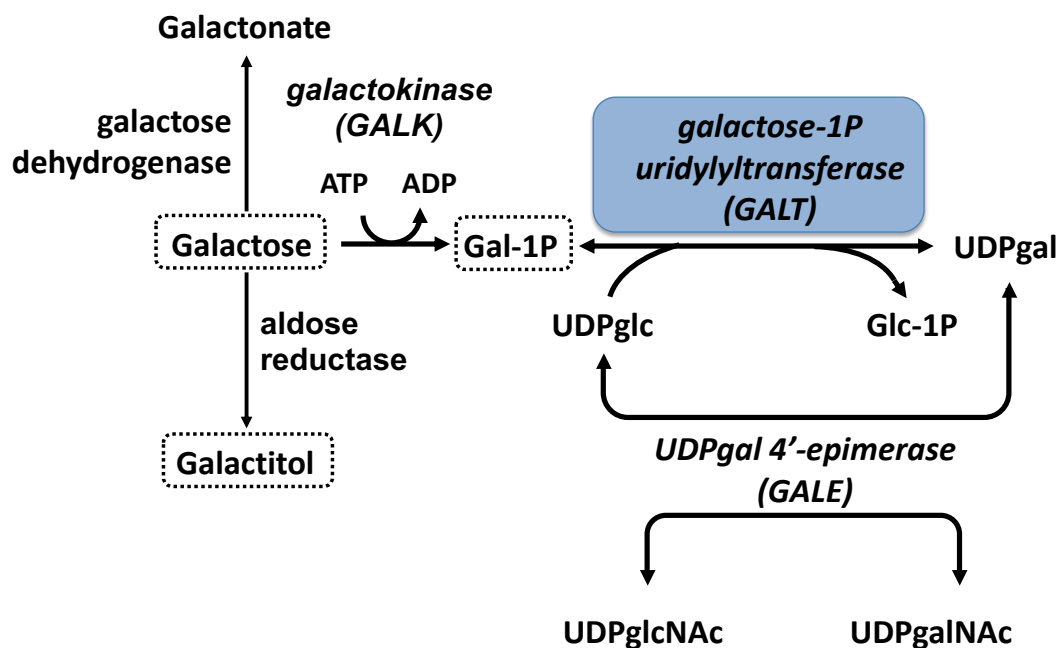


Figure 1. The Leloir Pathway of galactose metabolism. Figure is modified from Rasmussen et. al. 2020 (3).

CG affects approximately 1 in 30,000 – 60,000 newborns (5). If an infant with CG consumes lactose in their diet, the infant's health will rapidly deteriorate to a potentially life-threatening state. Infants suffering from CG and exposed to a lactose unrestricted diet can experience jaundice, sepsis, and failure to thrive, among other severe symptoms (4). Due to the implementation of newborn screening for CG, acute neonatal galactose toxicity can be avoided by placing an infant identified presymptomatically on a galactose restricted diet. However, even after early detection and dietary restriction, patients affected by CG commonly experience a number of long-term health complications including cognitive deficits, cataracts, motor deficits,

speech difficulties, growth delay, and primary ovarian insufficiency in female patients, among other issues. These symptoms demonstrate incomplete penetrance and variable expressivity, and generally present by mid-childhood (1). Most factors that modify outcome severity in CG remain poorly understood.

CG may be detected initially by elevated Gal-1P levels in erythrocytes but it is confirmed by the detection of absent or profoundly reduced GALT activity in erythrocytes (6). Genetic diagnosis is also possible. Management of CG consists of immediate dietary restrictions to minimize galactose consumption. Currently there is no cure for the disease, although treatments for specific symptoms of the disease, such as speech therapy, are available and can be beneficial. While dietary galactose restriction can substantially lower the accumulation of galactose metabolites, complete elimination of these metabolites is not possible for most patients due to the presence of endogenously produced galactose (7). Previous research remains inconclusive as to whether there is a causal relationship between any specific metabolite, such as galactitol or Gal-1P, and adverse patient outcomes. Additionally, metabolic markers such as erythrocyte Gal-1P may provide some insight into the accumulation of galactose metabolites in inaccessible tissues, such as the liver or brain; however, additional studies indicated there was no significant correlation with these markers and the severity of patient outcomes (1). The inconclusiveness of a causal role between a single metabolite and patient outcomes suggests that the cause may be a combination of multiple metabolites, or a combination of metabolites and other factors. As such, there is a critical need for additional research to clarify the mechanism of the disease.

Recent research has provided several opportunities for potential CG therapeutics. Pharmacologic inhibition of enzymes thought to synthesize metabolites that accumulate, such as Gal-1P and galactitol, enables the inhibition via delivery of small molecules. This approach

requires knowledge of causal metabolites linked to negative patient outcomes, and from the current understanding of CG this information remains inconclusive. In addition, if different metabolites are causal in different tissues, systemic treatment with any one inhibitor may modify some but not all adverse outcomes. Other options include pharmacologic chaperones, typically in the form of small molecules, that shift protein folding equilibrium towards the functional structure of GALT (7). Another alternative is attempting to restore GALT function by gene editing, viral gene therapy, or mRNA replacement, which has shown some success in multiple GALT-null animal models. Unlike other treatments, this approach aims to address the underlying cause of CG – the lack of functional GALT – rather than addressing the pathophysiology that results from inadequate GALT function (1). Although research continues to explore possible treatments, there remains a dire need for an effective therapeutic for patients currently living with CG.

The GALT-null Rat Model

GALT-null rats used in this project were descended from a gene edited GALT-null Sprague-Dawley rat produced in a collaboration between the Fridovich-Keil lab at Emory University and the Geurts lab at the Medical College of Wisconsin. CRISPR-Cas9 gene editing with non-homologous end joining was used to introduce a 2-base pair frameshift mutation, referred to as the M3 allele, in a male founder. The mutation introduced to the founder GALT-null male was confirmed using Sanger sequencing. The GALT-null male was then outbred to generate the homozygous *SD-GALT-M3* strain used in this project. GALT enzyme assays were performed to confirm GALT activity was below detectable limits in M3/M3 rat livers (3).

Further evaluation of the *SD-GALT-M3* strain demonstrated that the model presented the expected metabolite accumulations in multiple tissues. *GALT*-null pups euthanized within 24 hours of delivery and *GALT*-null pups euthanized at 20-23 days of age displayed much higher levels of galactose, galactitol, and Gal-1P than *GALT*+ pups in plasma, red blood cells, brain, liver, eyes, ovaries, and testes. *GALT*-null rats euthanized at 4-6 and 12-16 months showed metabolite levels that were still elevated, but significantly lower than the metabolite levels of their younger *GALT*-null counterparts (3).

AAV8 Gene Therapy

Adeno-associated virus (AAV) is a non-enveloped virus utilized as a gene delivery vector for therapeutic applications. AAVs can be engineered to deliver DNA to specific types of cells. For use as a gene therapy vehicle, recombinant AAV (rAAV) is employed to deliver a given transgene across the cell membrane and into the cell nucleus. rAAV lacks most viral DNA and therefore very rarely integrates into the host cell genome, and as a result, cannot replicate. After entry into the nucleus, the encoded transgene delivered by rAAV will form an episome within the nucleus. Because the episome does not replicate along with the host cell genome, as the cell undergoes replication or apoptosis, the episome will eventually be diluted out in a rapidly growing or remodeling tissue (8).

AAV8 is a serotype of AAV known to effectively transduce liver cells in rodents, dogs, and primates (9). In the past, AAV8 gene therapy was tested in liver-directed clinical trials for hemophilia B patients (10). The advantages of AAV8 for liver transduction include a high level of gene transfer via peripheral intravenous administration and a reduced number of antibodies in the human population compared to other serotypes. Despite these benefits, AAV8 gene therapy

still has limitations. Immune responses to AAV8 can substantially hinder transduction while also contributing to side effects of the therapeutic. This is particularly problematic in some applications when multiple administrations are required to restore gene function due to the non-replicating nature of the AAV8 episome. Although AAV8 is typically used for targeted transduction of the liver, past studies in rhesus monkeys showed some transduction was present in the brain, testes, muscle, kidney, heart, lung, and spleen (9). The use of a liver-specific promoter can help increase tissue specificity of transgene expression. Combining a liver-specific promoter with the established increased transduction of the AAV8 serotype has been implemented to both decrease immune response while also decreasing expression of the transgene in non-liver tissues (11).

AAV8 Administration to GALT-null Rats

This experiment aims to determine if intravenous (IV) administration of 5.0×10^{13} vg/kg AAV8-hAAT-HA-hGALT yields liver-specific expression of GALT. If expression is present, how much expression is achieved, and how long does the expression last? Additionally, if liver-specific GALT expression is present, does the expression lead to differences between galactose, galactitol, and/or Gal-1P metabolite levels in the liver, brain, and plasma?

To address these questions, the *SD-GALT-M3* strain was used to determine the efficacy of AAV8-hAAT-HA-hGALT GALT liver restoration. Viral stock was assembled from a plasmid and verified by VectorBuilder. Titer was determined via quantitative PCR (qPCR) and purity was assessed through SDS page followed by silver staining. The AAV8 encoding the hemagglutinin tagged (HA) human *GALT* cDNA was administered via tail-vein injection to rat pups. The viral vector also included a human alpha-1 antitrypsin (hAAT) liver-specific promoter

in an effort to decrease expression in tissues other than the liver. hAAT has been shown in the past to reduce autoimmunity in AAV8 therapies in multiple mouse studies (9, 12). Viral stock was preserved at -80 °C in PBS buffer (pH 7.4). The control AAV8-hAAT-GFP virus was obtained, tested, and stored in the same manner. Both viral stock solutions were diluted in sterile PBS just prior to administration to rat pups.

GALT-null (M3/M3) and wild-type (WT/WT) rat pups were administered intravenous treatment, or no treatment, within 48 hours after birth (P2). Treated GALT-null animals were injected with 5.0×10^{13} vg/kg AAV8-hAAT-HA-hGALT while control animals (GALT-null and wild-type rat pups) were administered 5.0×10^{13} vg/kg AAV8-hAAT-GFP via tail-vein injection. Additional GALT-null and wild-type control animals received no tail-vein injection at all.

Litters were weaned at 24 days of age to lab diet chow 5012 containing approximately 0.15% of calories from galactose. Rats were weighed daily from day 2 of age to day 34 of age (10 days post-weaning), after which they were weighed every 7 days up until euthanasia. Rats were euthanized and blood was collected; each rat was perfused with PBS prior to obtaining liver, brain, muscle, heart, kidney, eye, and gonad samples. Brain and liver samples intended for biochemistry were homogenized prior to being flash frozen in liquid nitrogen and stored at -80° C until processing.

GALT DC protein assays were performed on homogenized liver and brain samples to assess GALT activity. Metabolite extraction and quantification of galactose, galactitol, and Gal-1P was performed on liver, brain, and plasma samples (with no quantification of Gal-1P in plasma samples because it is a strictly intracellular metabolite). Specific GALT activity in liver was then compared to metabolite levels in all three tissue and blood samples to assess metabolic

efficacy of liver GALT restoration. Lastly, weight data and cataract scores were analyzed to determine the phenotypic efficacy of AAV8-mediated GALT liver restoration.

CHAPTER 2
LIVER GALT RESTORATION
BY AAV8-MEDIATED GENE THERAPY IN GALT-NULL RATS

Introduction

Past research has demonstrated that the use of the AAV8 serotype to provide targeted liver gene therapy yields encouraging results especially when used in combination with a liver specific promoter (9, 10, 11). This investigation aims to discern if administration of the AAV8-hAAT-HA-hGALT virus at 5.0×10^{13} vg/kg can restore meaningful levels of GALT activity in the liver while not restoring GALT to the brain in *SD-GALT-M3* rats. To evaluate the efficacy of the AAV8 virus, rats were harvested at the time points of 14, 30, 45, and 60 days post-injection (16, 32, 47, and 62 days of age). Rats were weighed prior to tissue collection and anesthetized using isoflurane prior to euthanasia by incision of the diaphragm. Blood samples from the left ventricle were obtained prior to PBS perfusion. Tissue samples collected were immediately flash frozen in 1.5 mL or 2.0 mL microfuge tubes in liquid nitrogen prior to storage at -80° C until further use. All procedures involving animals were conducted in a manner compliant with the Emory Institutional Animal Care and Use Committee (IACUC) protocol 201700095.

Methods

Blood Samples:

Blood samples were collected in sodium heparin BD Vacutainer tubes and placed on ice. For processing, blood samples were transferred to sterile 1.5 mL microfuge tubes. Microfuge tubes were spun at 4° C in an Eppendorf 5415D centrifuge at 4,800 rpm for 15 minutes. Afterwards, the separated plasma layer was aliquoted into sterile 1.5 mL microfuge tubes and immediately flash frozen in liquid nitrogen. The remaining RBCs were suspended in a 1:1

volume of 1X PBS (pH 7.4) prior to a second spin at 4,800 rpm for 15 minutes. The PBS layer was then discarded, and RBCs were aliquoted and flash frozen. Plasma and RBC aliquots were stored at -80° C until later use.

Table 1. Demographic Information of GALT Enzyme Assay Samples

FKRC	Genotype	Sex	Injection	Post Group
372.12	M3/M3	M	AAV8.hAAT.hGALT	14 days
372.08	M3/M3	F	AAV8.hAAT.hGALT	14 days
371.05	M3/M3	M	AAV8.hAAT.hGALT	14 days
371.04	M3/M3	F	AAV8.hAAT.hGALT	14 days
374.03	WT/WT	F	AAV8.hAAT.GFP	14 days
372.11	M3/M3	F	AAV8.hAAT.GFP	14 days
372.07	M3/M3	M	AAV8.hAAT.hGALT	30 days
372.06	M3/M3	F	AAV8.hAAT.hGALT	30 days
371.12	M3/M3	M	AAV8.hAAT.hGALT	30 days
371.01	M3/M3	F	AAV8.hAAT.hGALT	30 days
374.08	WT/WT	F	AAV8.hAAT.GFP	30 days
371.03	M3/M3	F	AAV8.hAAT.GFP	30 days
372.05	M3/M3	F	AAV8.hAAT.hGALT	45 days
372.03	M3/M3	M	AAV8.hAAT.hGALT	45 days
371.14	M3/M3	M	AAV8.hAAT.hGALT	45 days
371.02	M3/M3	F	AAV8.hAAT.hGALT	45 days
442.04	WT/WT	F	AAV8.hAAT.GFP	45 days
372.09	M3/M3	F	AAV8.hAAT.GFP	45 days
373.08	M3/M3	M	AAV8.hAAT.hGALT	60 days
373.07	M3/M3	F	AAV8.hAAT.hGALT	60 days
373.05	M3/M3	F	AAV8.hAAT.hGALT	60 days
373.04	M3/M3	M	AAV8.hAAT.hGALT	60 days
437.03	WT/WT	F	AAV8.hAAT.GFP	60 days
373.09	M3/M3	F	AAV8.hAAT.GFP	60 days

Animals shown are from a subset of all animals in this study. The full study included 6 – 9 animals per genotype and treatment group, but due to time constraints only a subset have been analyzed.

Protein Determination of Solid Tissue Lysates:

GALT DC protein assays were performed on liver and brain samples outlined in the protocol found in Rasmussen et. al. 2020, with adjustments of enzyme concentrations to ensure accurate quantification within the linear range (3). 6 animals were selected for each post-injection timepoint, consisting of 4 M3 hGALT (2 male, 2 female), 1 M3 GFP (female), and 1 WT GFP (female). 25-30 mg aliquots of frozen tissue were thawed and suspended in 100 μ L lysis buffer (EDTA-free, mini protease inhibitor cocktail pellet dissolved in 10 mL of 100 mM glycine, pH 8.7) and ground on ice using a Teflon micropestle. Samples were then centrifuged at 16,110 \times g for 5 minutes at 4°C. The supernatant was passed through a Micro Bio-Spin P-6 chromatography column to remove any endogenous metabolites and other small molecules.

A calibration curve was generated to quantify protein concentration within the P-6 flow through of each sample. 20 mg/mL BSA aliquots stored at -20°C were diluted to 1.5 mg/mL and serially diluted to create 5 standards of 1.5, 0.75, 0.375, and 0.1875 μ g/ μ L for use in the calibration curve. Liver samples were diluted 50-fold and brain samples were diluted 20-fold in lysis buffer for protein quantification. 4 replicates of 5 μ L sample or standard were added to a 96-well plate. 25 μ L of Bio-Rad DC Protein Assay Reagent A was added to each well followed by 200 μ L of Bio-Rad DC Protein Assay Reagent B and carefully mixed using a pipet to avoid the formation of bubbles. The 96-well plate was then incubated in dark conditions for 15 minutes before analysis by an EL808 Ultra Microplate Reader (Bio-Tek Instruments, Inc). The data provided were used to generate a linear calibration curve to determine protein quantification within each sample. The protein concentration in the sample was diluted to the appropriate final concentration in microfuge tubes for the enzyme assay reaction (Table 2). The final liver protein concentration was repeatedly increased for assays performed on samples obtained from later time points due to the observation that GALT activity decreases with the animals' increasing age in

both treated GALT-null and wild-type rats; this trend was also observed in previous studies (3, 13). Final protein concentrations for brain samples were held at 40 μg because no detectable GALT activity was expected in M3 brain samples; previous experiments also showed that exceeding this amount did not yield different results from brain assays performed at final concentrations of 40 μg of protein (3, 13).

Table 2: Final Dilutions Used in GALT Enzyme Assay

Post Group	Tissue	Group	Amount of Protein Used (μg)
14 days	Liver	WT GFP	2
		M3 hGALT	0.5
		M3 GFP	10
	Brain	WT GFP	20
		M3 hGALT	40
		M3 GFP	40
30 days	Liver	WT GFP	2
		M3 hGALT	14
		M3 GFP	10
	Brain	WT GFP	20
		M3 hGALT	40
		M3 GFP	40
45 days	Liver	WT GFP	2
		M3 hGALT	30
		M3 GFP	10
	Brain	WT GFP	20
		M3 hGALT	40
		M3 GFP	40
60 days	Liver	WT GFP	5
		M3 hGALT	30*
		M3 GFP	10
	Brain	WT GFP	20
		M3 hGALT	40
		M3 GFP	40

*One 60-day M3 hGALT liver sample had its protein concentration lowered to 13 μg due to displaying exceptionally high GALT activity after repeated attempts of the assay.

GALT Activity Assays:

30 μL of each sample was transferred to a microfuge tube containing 20 μL of +Gal-1P premix (312.5 μL of 1M glycylglycine pH 8.7, 20 μL of 100mM UDP-glucose (UDPglc), 40 μL of 100mM Gal-1P, and 627.5 μL Milli-Q H_2O) or 20 μL of -Gal-1P premix (312.5 μL of 1M glycylglycine pH 8.7, 20 μL of 100mM UDPglc, and 667.5 μL Milli-Q H_2O). Two replicates of +Gal-1P and one replicate of -Gal-1P solutions were created with final volumes of 50 μL . The resulting solution was gently vortexed to initiate the reaction and incubated for 30 minutes in a water bath at 37° C. After incubation, samples were immediately placed on ice, quenched with 450 μL ice-cold Milli-Q water, and vortexed at the maximum setting to halt the reaction. The solutions were passed through 0.22 μm Costar Spin-X centrifuge tube filters at 4,000 $\times g$ for 4 minutes at 4° C and stored at -80° C until HPLC analysis.

HPLC Analysis:

Substrates and products of the reaction were separated and quantified using a Dionex ICS-5000 HPLC system. Samples were passed through a Dionex Borate Trap (trap column, 4 x 50 mm), a Dionex Amino Trap (trap column, 4 x 50 mm), and finally a Dionex CarboPac PA10 (analytical column, 4 x 250 mm) sequentially. Mobile phase buffers consisted of 15 mM NaOH (buffer A) and 50 mM NaOH with 1 M NaOAc (Buffer B). The PA10 column used a flow rate of 1.0 mL/min with varying buffer ratios as the sample was eluted (Table 3). Autosampler trays were chilled at 4° C prior to loading of samples, and injection volume for all samples and standards was 20 μL .

Table 3. PA10 Column Enzyme Assay Buffer Gradient Cycle

Time (min)	Buffer A%	Buffer B%
-2.0	85	15
5.0	85	15
10.0	75	25
27.5	30	70
37.0	30	70
39.0	85	15
44.0	85	15

A 1x stock solution of GALT substrates and products was diluted to obtain a standard curve for the PA10 sequence from 0.1x, 0.5x, and 1x dilutions. The GALT 1x 10 mL stock solution consisted of 100 μ L 10 mM Gal-1P, 100 μ L of 10 mM Glc-1P, 150 μ L of 20 mM UDPgal, 300 μ L of 10 mM UDPglc, and 9350 μ L MilliQ H₂O. The standard curve was used to measure amounts of UDPgal and UDPglc in eluent in pmol. Enzyme activity for each sample was calculated in pmol of product formed per μ g total protein per minute of reaction time (pmol UDPgal/ μ g protein/min).

Results

GALT activity in the liver showed a general increase in M3 hGALT rats compared to their M3 GFP counterparts. This difference was most prominent at 14 days post-injection (Figure 2) and continued to become less pronounced further from the day of injection.

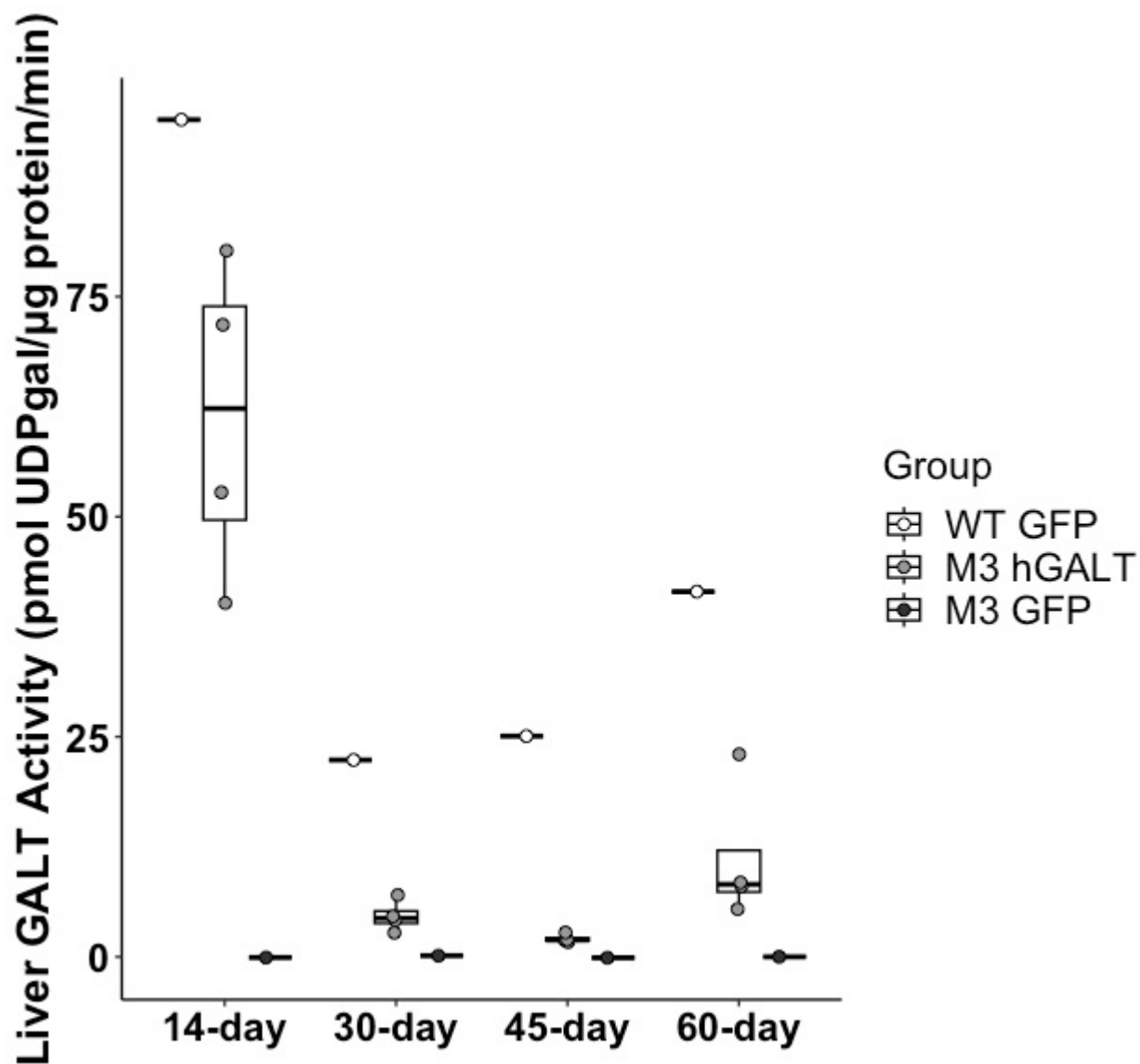


Figure 2. Liver GALT activity is shown for all post-injection tissue collection dates. At each collection point, data consist of 1 WT GFP, 4 M3 hGALT, and 1 M3 GFP sample.

At 30 days post-injection or beyond, WT GFP GALT activity also shows a large decrease, never surpassing 50% of the 14 days post-injection GALT activity.

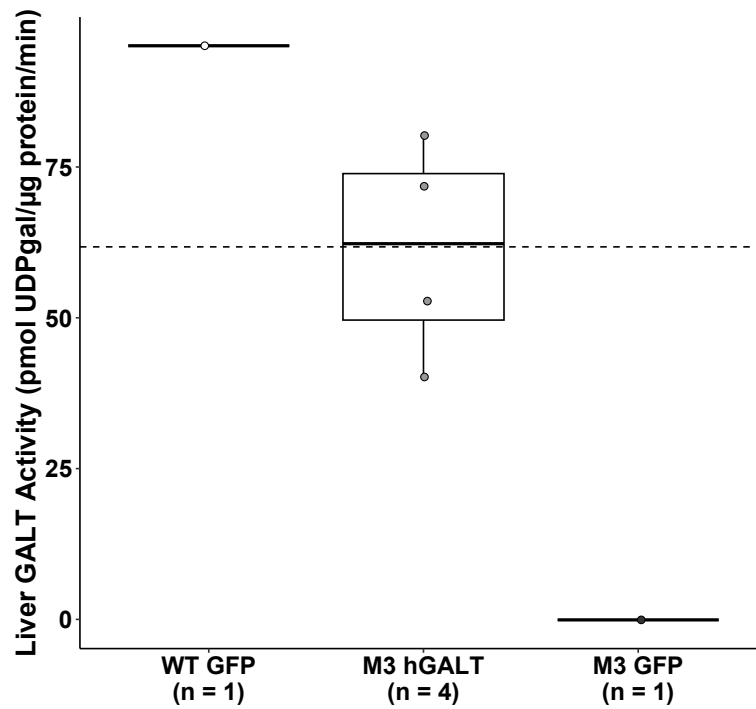


Figure 3. Liver GALT activity shown for livers collected 14 days post-injection. Dashed line represents average liver GALT activity from WT PBS injected animals collected 14 days post-injection from a previous study (n =5) (13).

Across all 3 groups, liver GALT activity was highest at 14 days post-injection. This finding is consistent with previous research where liver GALT activity in both wild-type and treated GALT-null rats decreased with age (3).

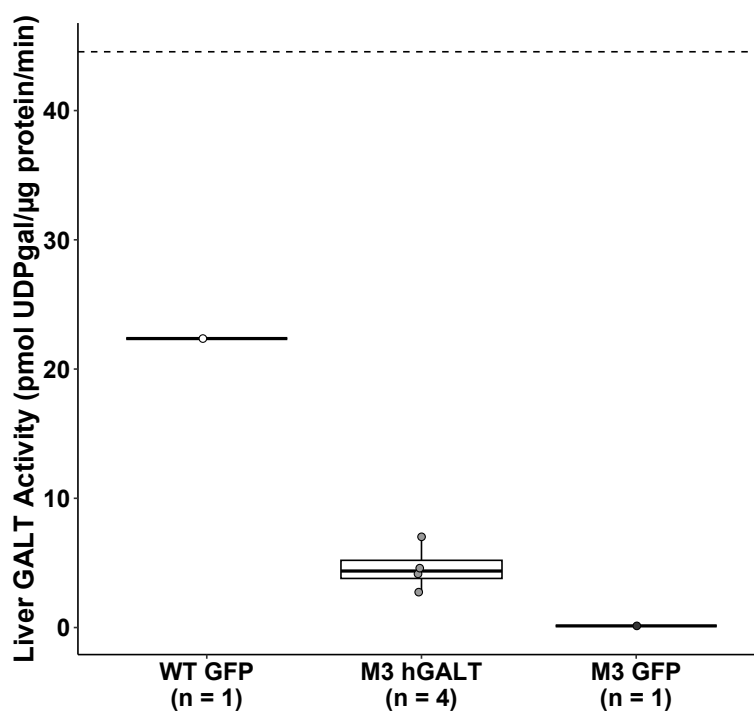


Figure 4. Liver GALT activity shown for livers collected 30 days post-injection. Dashed line represents average liver GALT activity from WT PBS injected animals collected 30 days post-injection from a previous study (n =9) (13).

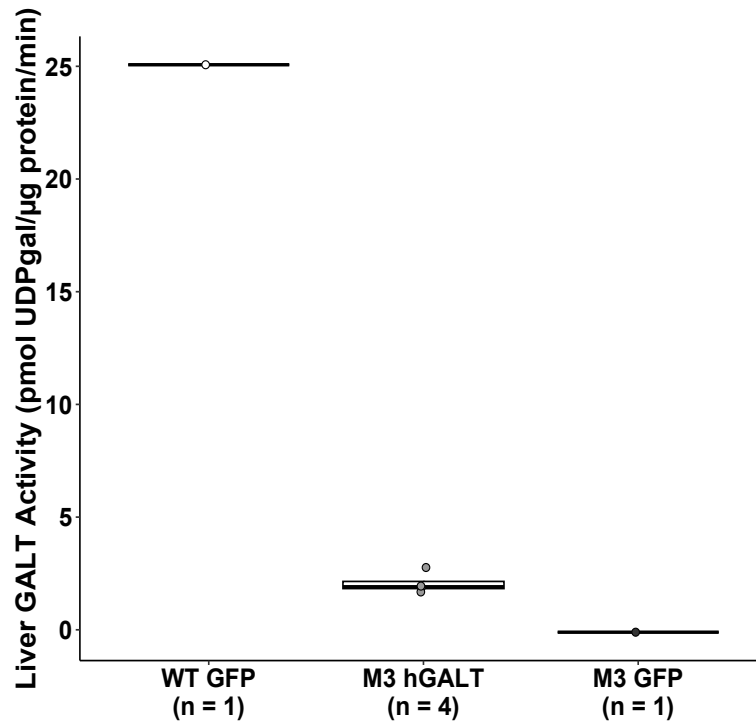


Figure 5. Liver GALT activity shown for livers collected 45 days post-injection.

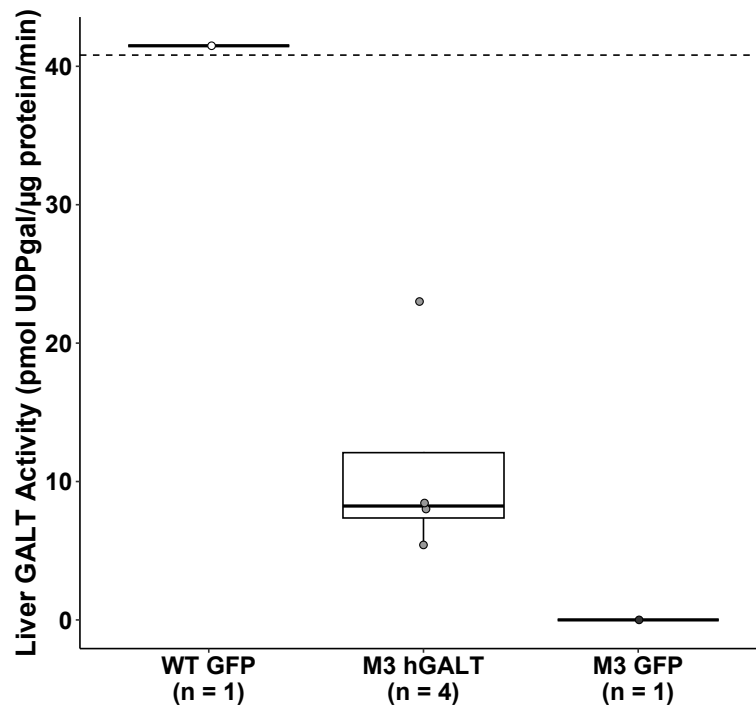


Figure 6. Liver GALT activity shown for livers collected 60 days post-injection. Dashed line represents average liver GALT activity from WT PBS injected animals collected 60 days post-injection from a previous study (n=3) (13).

GALT activity in the brain was below detectable limits in both M3 hGALT and M3 GFP groups at all post-injection time points that tissues were collected. This is consistent with the expected liver-specific transgene expression associated with AAV8 virus and the hAAT promoter (9, 12, 11).

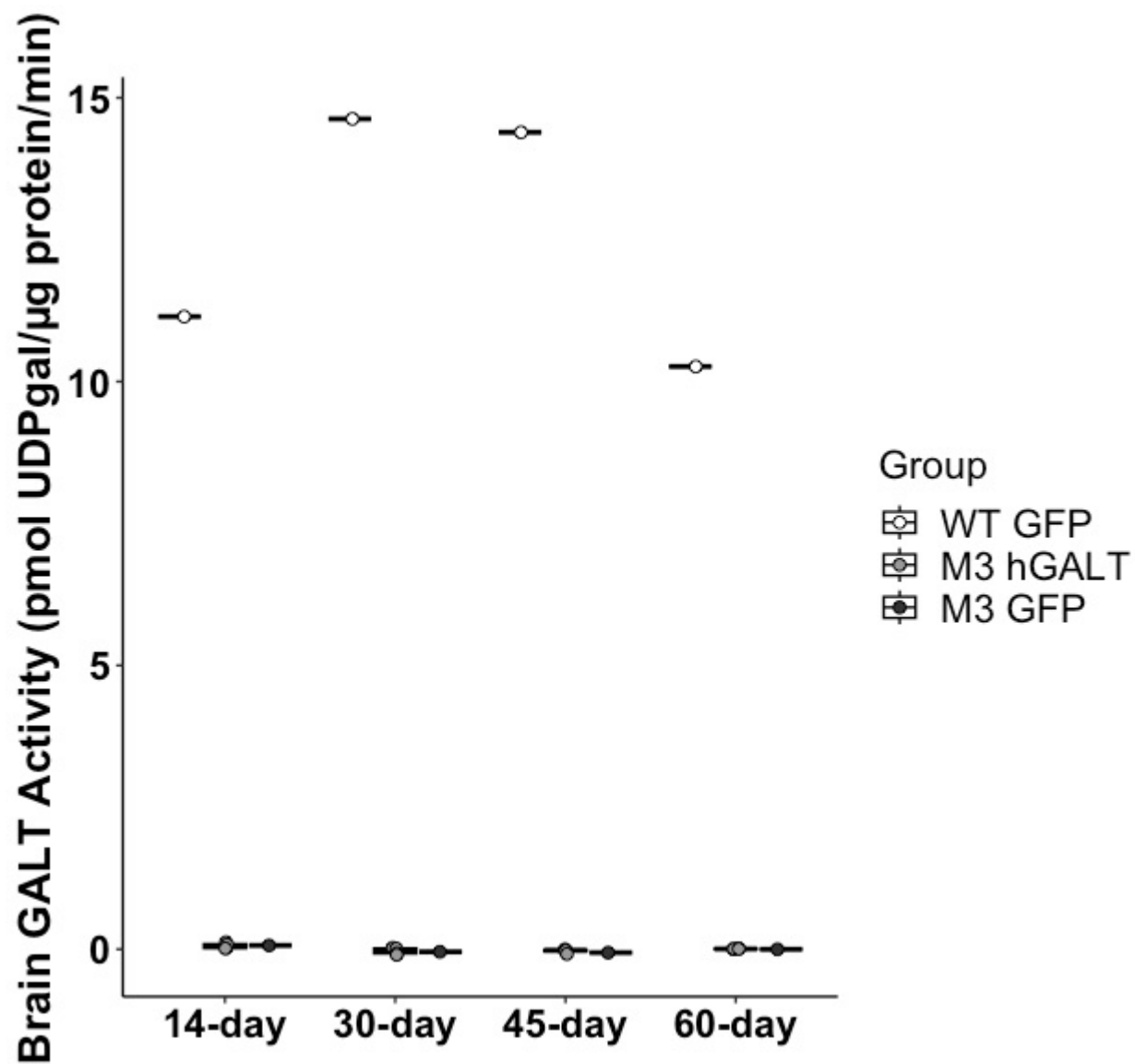


Figure 7. Brain GALT activity is shown for all post-injection tissue collection dates. At each collection point, data consist of 1 WT GFP, 4 M3 hGALT, and 1 M3 GFP sample.

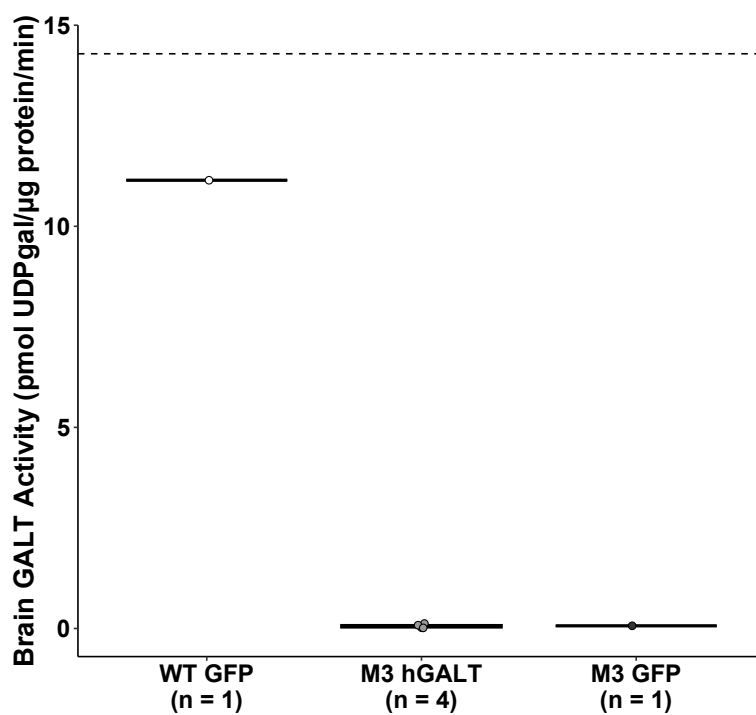


Figure 8. Brain GALT activity shown for brains collected 14 days post-injection. Dashed line represents average brain GALT activity from WT PBS injected animals collected 14 days post-injection from a previous study (n = 6) (13).

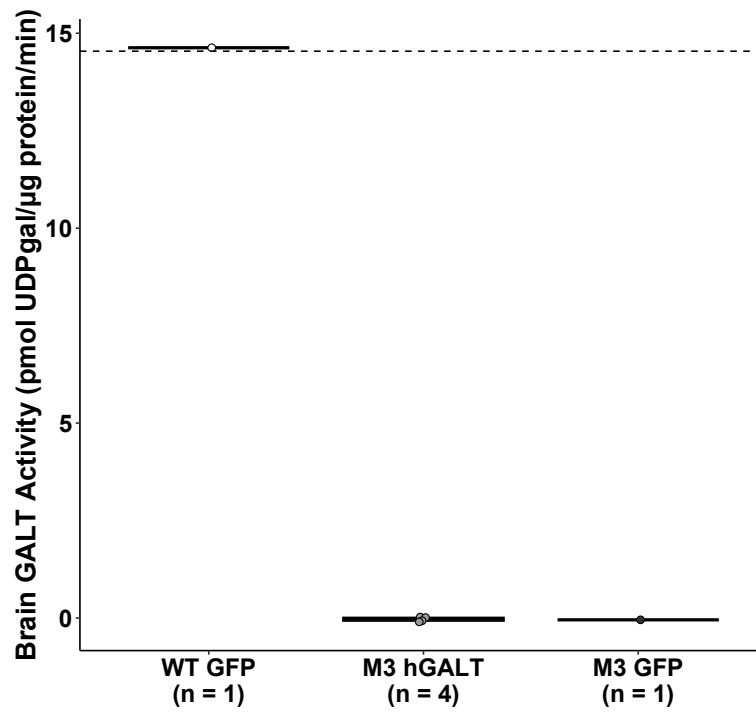


Figure 9. Brain GALT activity shown for brains collected 30 days post-injection. Dashed line represents average brain GALT activity from WT PBS injected animals collected 30 days post-injection from a previous study (n = 6) (13).

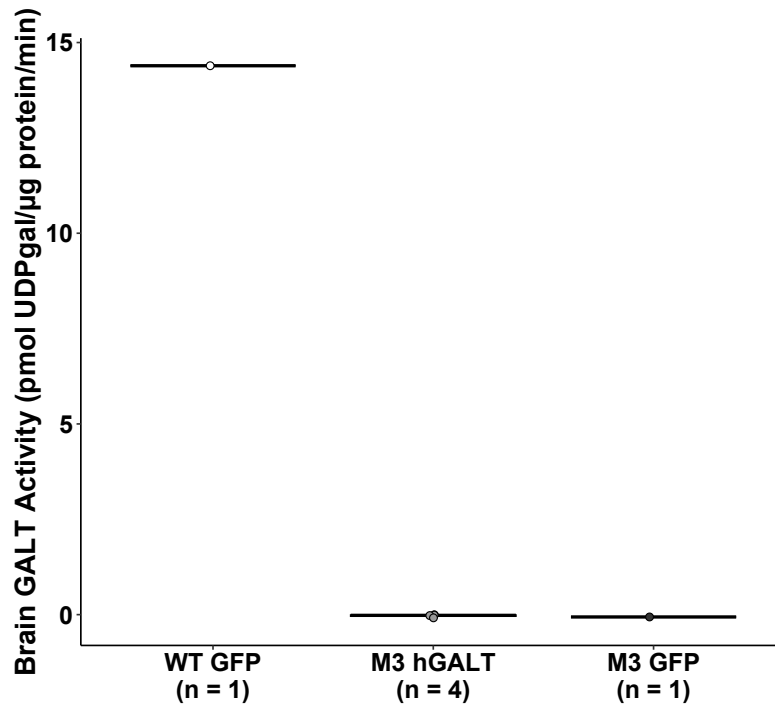


Figure 10. Brain GALT activity shown for brains collected 45 days post-injection.

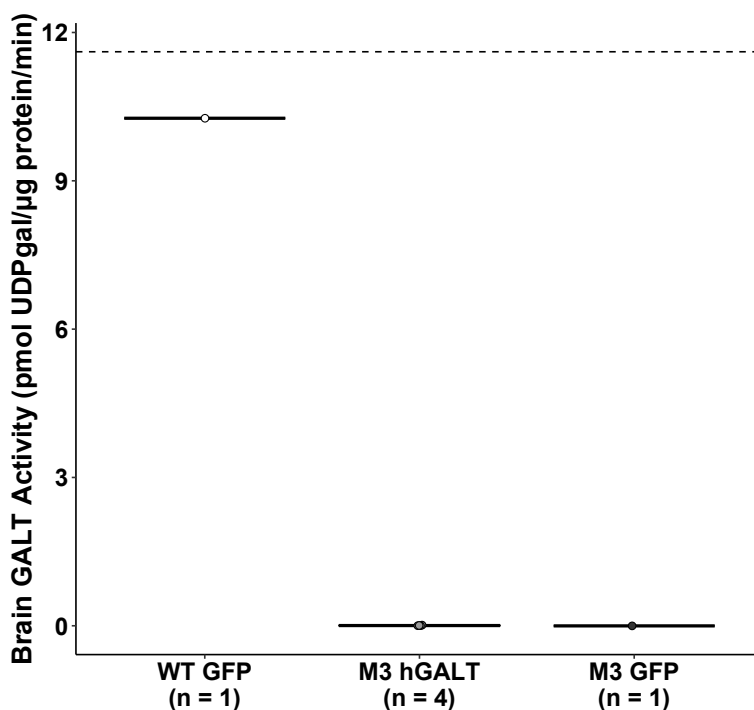


Figure 11. Brain GALT activity shown for brains collected 60 days post-injection. Dashed line represents average brain GALT activity from WT PBS injected animals collected 60 days post-injection from a previous study (n = 3) (13).

Discussion

GALT assay data from liver and brain indicate a degree of GALT restoration in the liver without GALT restoration in the brain in M3 hGALT rats. WT GFP and M3 hGALT rats show highest liver GALT activity at the earliest collection date of 14 days post-injection (Figures 2, 3). M3 GFP rats present with liver GALT activity below detectable limits at all time points as predicted from earlier GALT-null rat studies (3, 13). A pattern of M3 hGALT rats displaying greater liver GALT activity than M3 GFP rats exists throughout all time points (Figure 2). Liver GALT activity decreased in the WT GFP group from 14 days post-injection to 30 days post-injection. However, the liver GALT activity decrease in the treated M3 hGALT group declines substantially more between these two collection dates when compared to the difference in liver

GALT activity observed in the WT GFP group (Figures 3, 4). As rats develop more rapidly than humans, reaching sexual maturity at around 8 weeks of age, a possible explanation for this rapid decline could be the substantial growth of the rat pup from 16 to 32 days of age (14 to 30 days post-injection) (14). Due to the AAV8 episome's lack of integration into the host genome, as the liver of a rat pup rapidly grows and develops, the overall proportion of AAV8 transduced cells relative to unmodified cells likely decreases as the rat grows. An alternative explanation of this observation could be AAV8 transduced hepatocytes are being perpetually destroyed as the liver matures, decreasing the overall amount of AAV8 transduced hepatocytes in the liver (8). Despite this decrease in liver GALT activity, the remaining amount may still reduce levels of elevated metabolites characteristic of CG as discussed in Chapter 3.

Results from brain GALT assays demonstrate brain GALT activity in treated M3 hGALT and M3 GFP rats consistently remains below detectable limits at all time points. In contrast, the WT GFP group shows sustained brain GALT activity between 10 – 15 pmol UDPgal/ μ g protein/min at 14, 30, 45, and 60 days post-injection (Figure 7). These results indicate the AAV8-hAAT-HA-hGALT virus did not express the *GALT* transgene in brain cells in treated M3 hGALT rats.

Statistical methods could not be applied to the results presented in this chapter because of the small sample size in each comparison group. Due to time limitations and the restriction of only being able to perform the procedure on six samples at a time, only one WT GFP and one M3 GFP sample were analyzed per time point. Previous data from Daenzer et. al. 2022 was displayed in addition to data from this investigation to supplement the small n of WT GFP observations. Mean GALT activity for WT PBS injected rats was shown in several of the figures to provide an additional indicator of WT rat GALT activity in liver and brain tissues (13)

(Figures 3, 4, 6, 8, 9, 11). Although Figures 2, 3, and 7 show notable differences between the single WT GFP rat GALT activity and average GALT activity from WT PBS animals, the WT PBS GALT activity standard deviations reported at these time points were ± 10.96 , 10.72 , and 3.87 pmol UDPgal/ μ g protein/min respectively, indicating noticeable variation among wild-type rats (13). As the AAV8-hAAT-GFP virus does not contain the GALT transgene, the WT GFP group was deemed comparable to WT PBS injected rats. Even so, small sample size among WT GFP, treated M3 hGALT, and M3 GFP groups remains a significant limiting factor in this investigation. Overall, the GALT assay results suggest successful transduction of AAV8-hAAT-HA-hGALT into the livers of M3 hGALT animals without expression in the brain. Further from the day of injection, treated M3 hGALT rats show decreased liver GALT activity especially between 14 and 30 days post-injection.

CHAPTER 3
METABOLIC EFFICACY OF LIVER GALT RESTORATION
BY AAV8-MEDIATED GENE THERAPY IN GALT-NULL RATS

Introduction

Numerous studies in human patients with classic galactosemia suggest a link between the accumulation of metabolites within the Leloir Pathway of galactose metabolism with adverse patient outcomes (1, 15, 16). Red blood cell (RBC) Gal-1P is also used as a common biomarker followed in patients for CG detection, patient dietary compliance, and as a proxy for metabolic status in inaccessible tissues. Although some doubt has been cast upon the use of RBC Gal-1P as a tool to predict metabolism in tissues such as the liver and brain, determining the metabolic efficacy of AAV8-mediated GALT liver restoration is critical to assessing the effects of the gene therapy treatment in GALT-null rats (3). Previous research utilizing an scAAV9-CBh-hGALT administered at 2.5×10^{13} vg/kg via tail-vein injection found strong transgene expression in both the liver and brain of GALT-null rats. This transgene expression further resulted in near-complete metabolic rescue in early development leading up to young adulthood in addition to reducing the symptoms of cataracts and pre-pubertal growth delay in GALT-null rats (13). To evaluate the metabolic efficacy of the AAV8 treatment, galactose, galactitol, and Gal-1P were quantified in liver and brain samples, while only galactose and galactitol were quantified in plasma due to Gal-1P being an intracellular metabolite.

Methods

Sample Collection:

Liver, brain, and blood samples from the left ventricle were collected from the same animals used for GALT enzyme assays. Additional samples from animals enrolled in this study

were used to supplement metabolite analysis of animals tested for liver and brain GALT activity. These samples were obtained from other rats of the same genotype, treatment group, and post-injection collection dates to increase the available sample size. Rats were euthanized using the same procedure as described in Chapter 2. Livers and brains were removed from the animals and homogenized using sterile razor blades prior to a handheld OMNI THb International tissue homogenizer. 100 – 110 mg of tissue were aliquoted into 1.5 mL microfuge tubes and immediately flash frozen in liquid nitrogen prior to storage at -80°C until further processing. Plasma blood samples were obtained using the same procedure described in Chapter 2. 100 μL plasma aliquots were placed in 1.5 mL microfuge tubes before flash freezing in liquid nitrogen and storage at -80°C .

Metabolite Extraction:

Metabolites were extracted using a protocol similar to Rasmussen et. al. 2020 (3). Tissue and plasma aliquots were thawed on ice. 125 μL of 4°C MilliQ water was added to the tissue aliquots. Liver and brain samples were ground on ice using a Teflon micropestle. After tissues were homogenized, 250 μL 100% HPLC grade MeOH and 500 μL HPLC grade CHCl_3 stored at -20°C were added to the microfuge tube. Samples were then vortexed at the maximum setting for 45 minutes at 4°C . Microfuge tubes were transferred to an Eppendorf 5415D centrifuge and spun at 2000 rpm for 20 minutes at 4°C . Samples were immediately transferred to ice and the top aqueous layer was moved to a second microfuge tube placed in ice. A second extraction was then performed with the addition of 125 μL 100% HPLC grade MeOH and 125 μL MilliQ water. Samples were vortexed again at maximum setting for 5 minutes at 4°C prior to another 2000 rpm spin for 20 minutes at 4°C . The second top aqueous layer was transferred to the microfuge

tube holding the extracted metabolites from the first round of extraction. Samples were then placed in an Eppendorf Vacufuge speedvac and dried with no heat for 1.5 – 3 hours depending on the metabolite source. After a dried metabolite pellet was obtained, the pellet was resuspended in 200 μ L of 4° C MilliQ water and rested for 10 minutes at 4° C. The resuspended metabolites were then mixed with a pipette and passed through 0.22 μ m Costar Spin-X centrifuge tube filters at 4,000 xg for 4 minutes at 4° C. Filtered metabolites were stored at -80° C until HPLC analysis.

HPLC Analysis:

Metabolites were separated and quantified using either a Dionex ICS-5000 HPLC system or Dionex ICS-6000 HPLC system. Quantification of Gal-1P was performed on the PA10 column described in Chapter 2. For metabolite separation, a different PA10 buffer ratio variation was used as outlined in Table 4 with a constant flow rate of 0.4 mL/min. Galactose, galactitol, and glucose were quantified by passing samples sequentially through a Dionex CarboPac MA1 (guard column, 4 x 50 mm), a Dionex Amino Trap (trap column, 4 x 50 mm), and lastly a Dionex CarboPac MA1 (analytical column, 4 x 250 mm). MA1 column mobile phase buffers consisted of 1 M NaOH (buffer A) and 15 mM NaOH (buffer B). Samples were eluted at a constant flow rate of 0.8 mL/min and buffer ratios were varied as shown in Table 5. Autosampler trays used for the ICS-5000 were chilled at 4° C prior to use; trays used in the ICS-6000 instrument were temperature controlled throughout the injection process. Injection volume for all samples and standards used was 20 μ L.

Table 4. PA10 Column Metabolite Buffer Gradient Cycle

Time (min)	Buffer A%	Buffer B%
-5.0	90	10
1.0	90	10
30.0	35	65
52.0	35	65
54.0	90	10

Table 5. MA1 Column Metabolite Buffer Gradient Cycle

Time (min)	Buffer A%	Buffer B%
-5.0	30	70
43.0	30	70
45.0	70	30

To obtain a standard curve for Gal-1P, a 10x stock solution of PA10 standard was diluted to 1x, 5x, and 10x concentrations. The PA10 10x 10 mL stock solution was formed from 50 μ L 10 mM galactose, 50 μ L 10 mM glucose, 400 μ L of 100 mM Gal-1P, 100 μ L of 10 mM Glc-1P, 100 μ L of 10 mM Fruc-1P, 50 μ L of 10 mM Fruc-6P, 100 μ L of 10 mM galactonate, 50 μ L of 20 mM UDPgal, 100 μ L of 10 mM UDPglc, 5 μ L of 20 mM UDPgalNac, 10 μ L of 10 mM UDPglcNac, and 8885 MilliQ H₂O. A linear standard curve was used to measure amounts of Gal-1P in liver and brain eluent. 10x stock solution of MA1 standard was diluted to 1x, 5x and 10x concentrations to quantify galactose, galactitol, and glucose in all samples. The 10x MA1 10 mL stock solution consisted of 50 μ L of 10 mM myo-inositol, 100 μ L of 10 mM galactitol, 50 μ L 10 mM glucose, 50 μ L of 10 mM galactose, and 9750 μ L MilliQ H₂O. Extracted metabolites were diluted according to tissue. Liver samples were diluted 10-fold, brain samples were diluted 2-fold, and plasma metabolites remained undiluted. Following quantification, metabolites were calculated in pmol/mg of solid tissue or pmol/ μ L of plasma.

Results

Due to time constraints, only a subset of the total available samples could be analyzed. Pairwise comparisons using Wilcoxon rank sum exact tests were performed to determine if there were significant differences in median metabolite levels between M3 hGALT and M3 GFP groups ($\alpha = 0.05$). These statistical tests serve only as a preliminary analysis of the current data due to the limited sample size at each post-injection collection date. Significant p -values are indicated in figure captions with an asterisk (*).

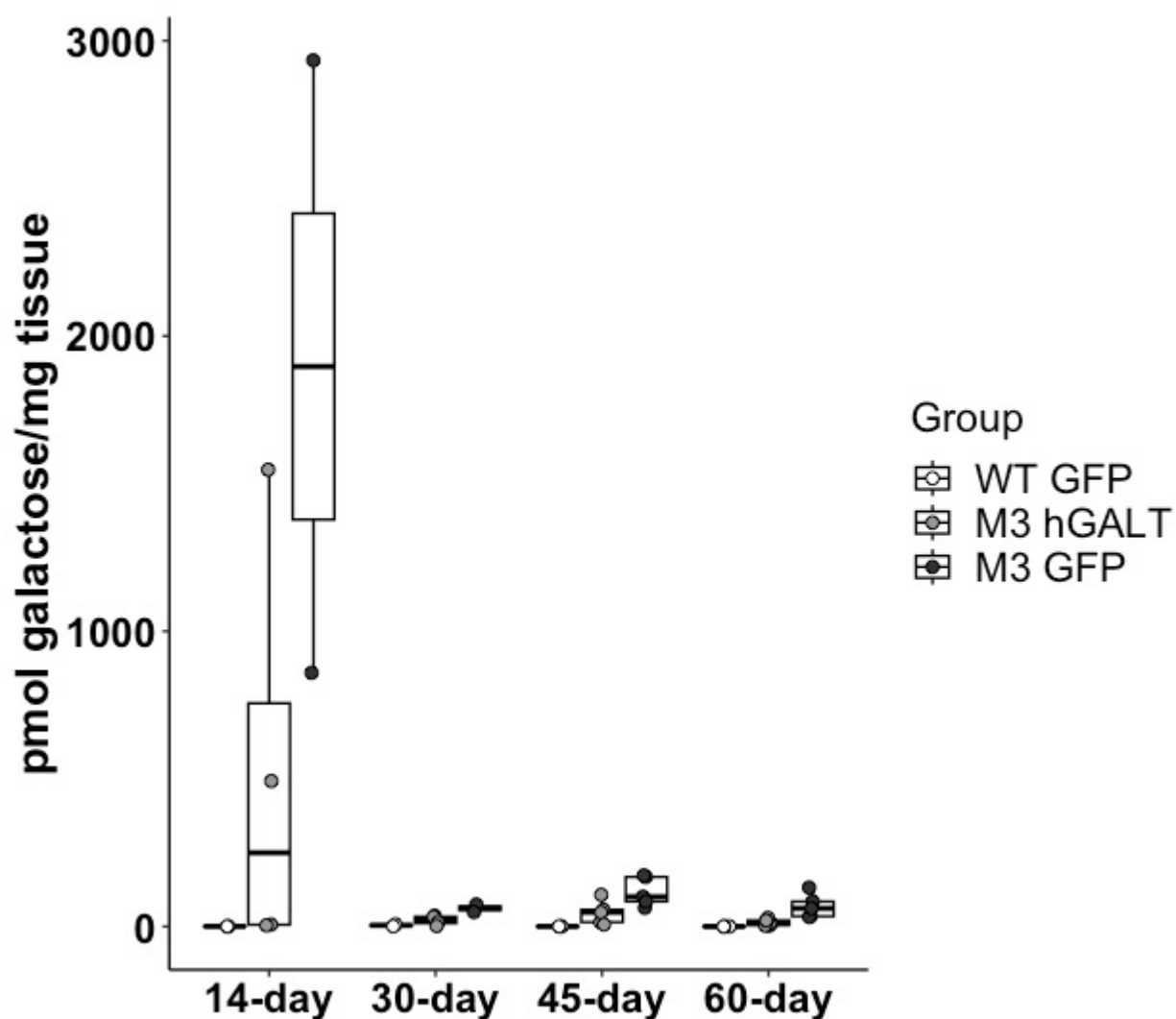


Figure 12. Liver galactose levels are shown for all post-injection tissue collection dates. At each collection point, data consist of 2 – 3 WT GFP, 4 – 8 M3 hGALT, and 1– 5 M3 GFP samples. At each timepoint, the WT GFP and M3 GFP groups contain 1 WT untreated and 1 M3 untreated animal respectively.

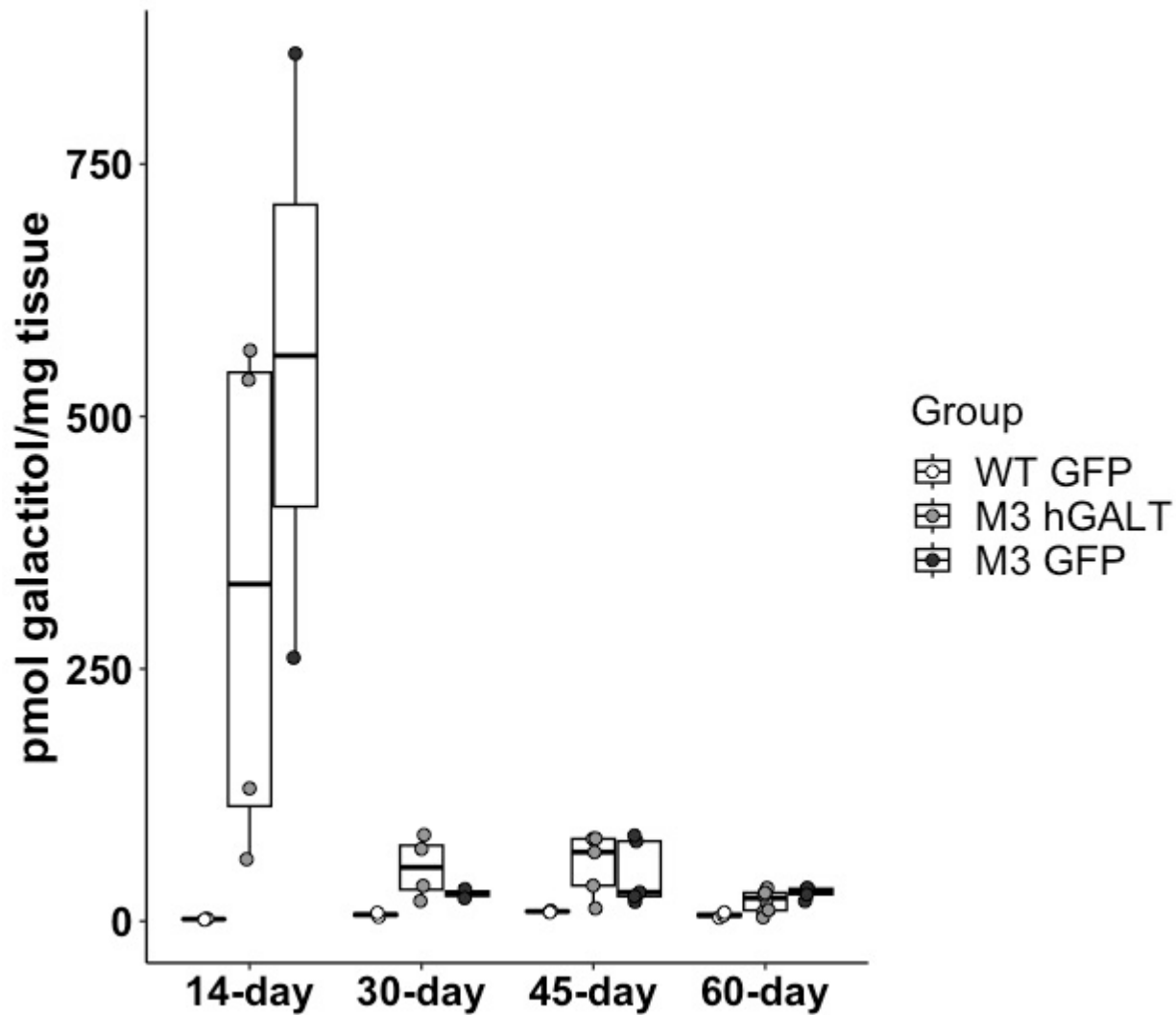


Figure 13. Liver galactitol levels are shown for all post-injection tissue collection dates. At each collection point, data consist of 2 – 3 WT GFP, 4 – 8 M3 hGALT, and 1– 5 M3 GFP samples. At each timepoint, the WT GFP and M3 GFP groups contain 1 WT untreated and 1 M3 untreated animal respectively.

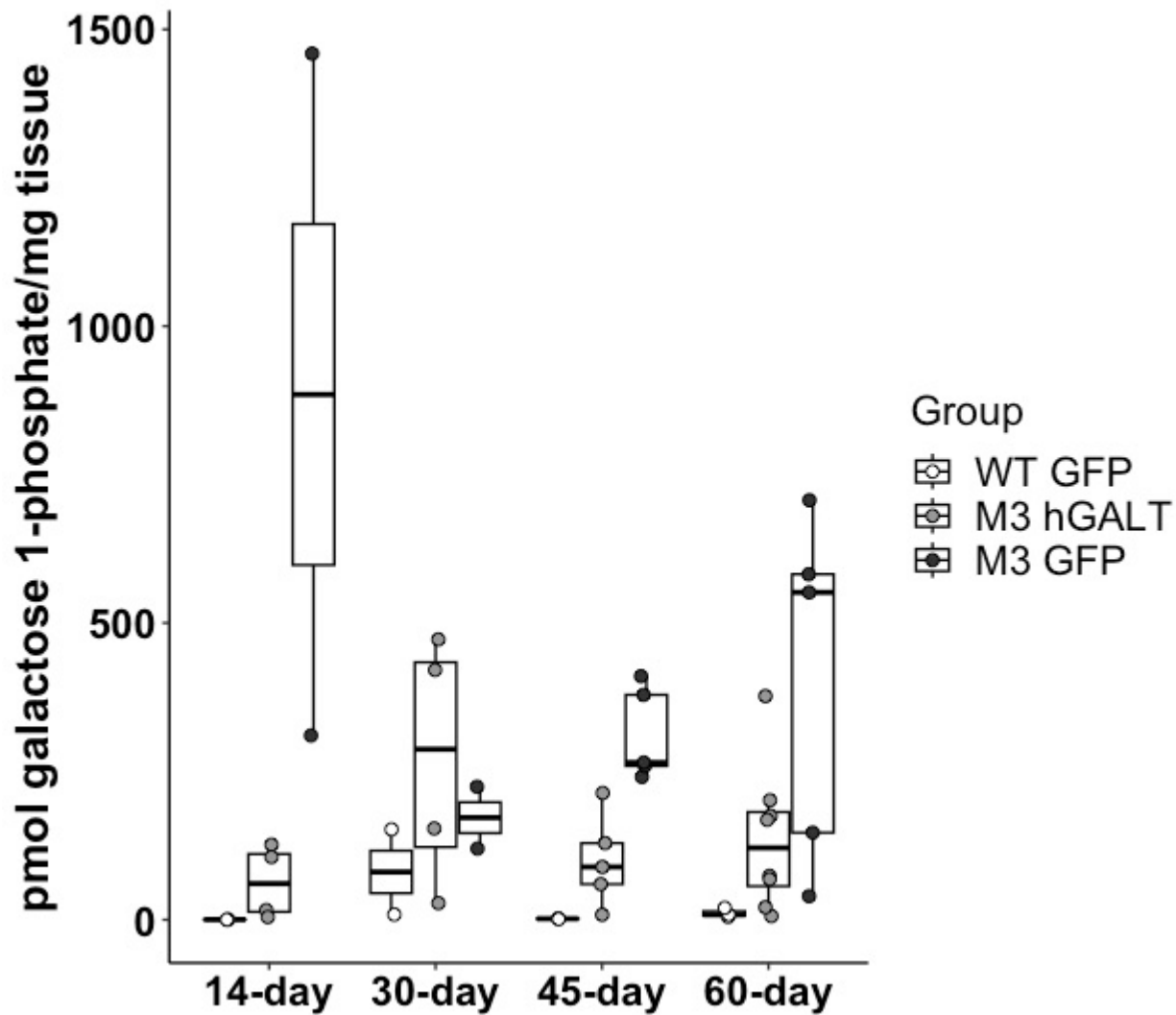


Figure 14. Liver Gal-1P levels are shown for all post-injection tissue collection dates. At each collection point, data consist of 2 – 3 WT GFP, 4 – 8 M3 hGALT, and 1 – 5 M3 GFP samples. At each timepoint, the WT GFP and M3 GFP groups contain 1 WT untreated and 1 M3 untreated animal respectively. Pairwise comparisons using Wilcoxon tests between M3 GFP and M3 hGALT: 14 days post-injection $p = 0.13$, 30 days post-injection $p = 0.80$, 45 days post-injection $p = 0.0079^*$, and 60 days post-injection $p = 0.17$.

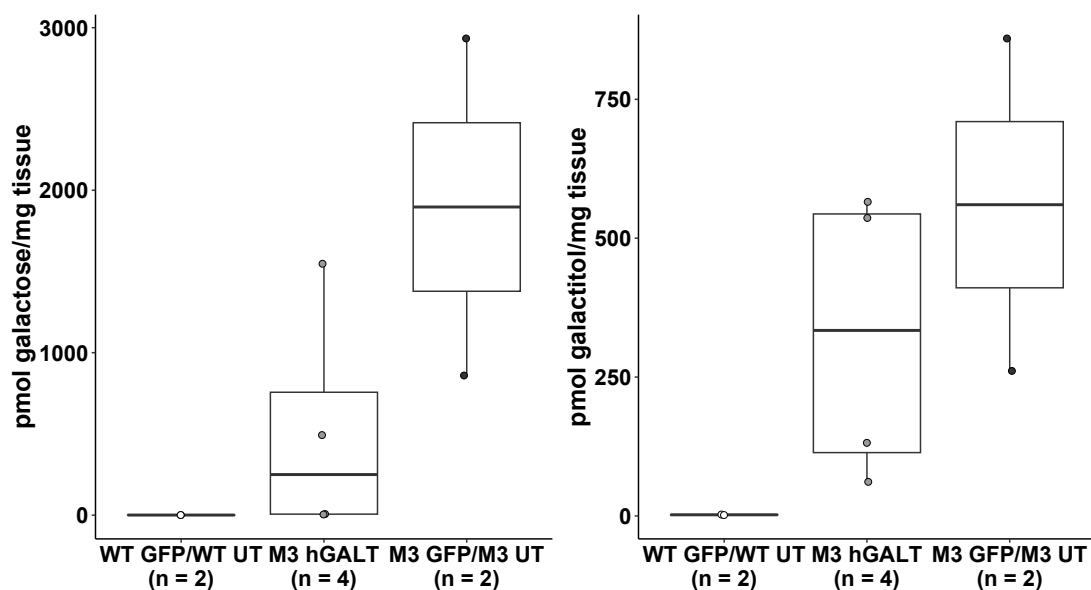


Figure 15. Liver galactose and galactitol levels are shown for livers collected 14 days post-injection. Pairwise comparisons using Wilcoxon tests between M3 GFP and M3 hGALT galactose yielded $p = 0.27$ and comparing galactitol $p = 0.53$; however, the small size of the dataset analyzed limits the utility of these comparisons.

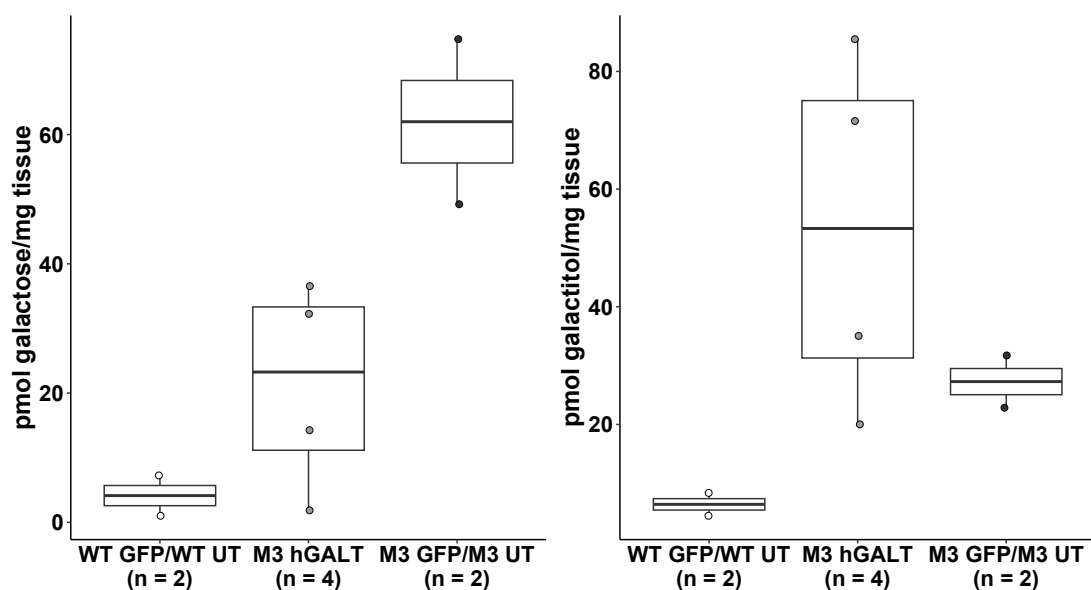


Figure 16. Liver galactose and galactitol levels are shown for livers collected 30 days post-injection. Pairwise comparisons using Wilcoxon tests between M3 GFP and M3 hGALT galactose yielded $p = 0.13$ and comparing galactitol $p = 0.53$.

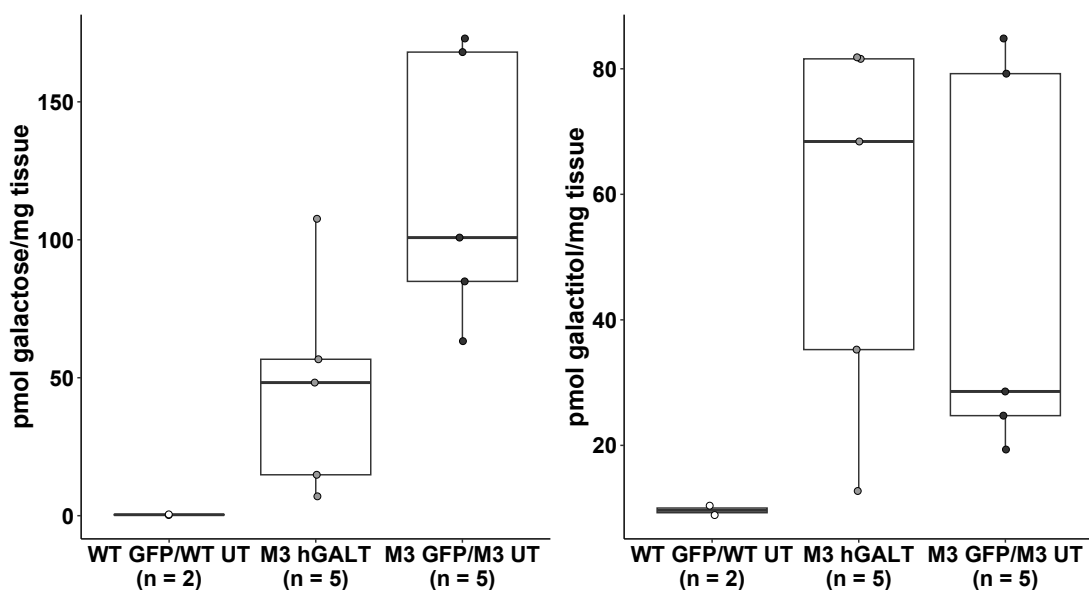


Figure 17. Liver galactose and galactitol levels are shown for livers collected 45 days post-injection. Pairwise comparisons using Wilcoxon tests between M3 GFP and M3 hGALT galactose yielded $p = 0.056$ and comparing galactitol $p = 0.84$.

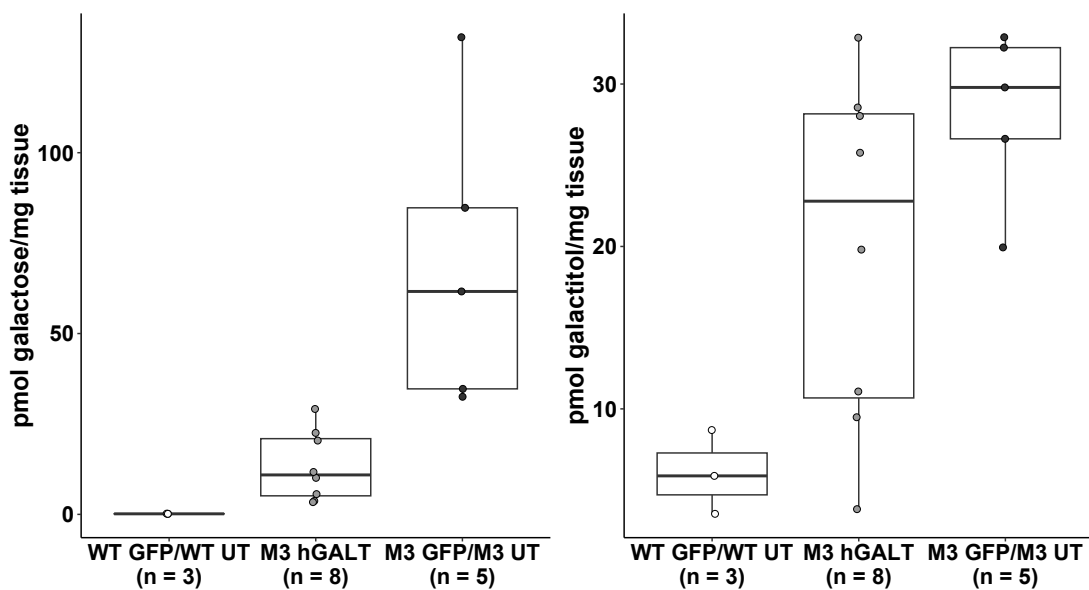


Figure 18. Liver galactose and galactitol levels are shown for livers collected 60 days post-injection. Pairwise comparisons using Wilcoxon tests between M3 GFP and M3 hGALT galactose yielded $p = 0.0016^*$ and comparing galactitol $p = 0.13$.

Metabolite levels in the liver show a general decrease in M3 hGALT rats compared to their M3 GFP counterparts. This difference was most noticeable at 14 days post-injection (Figures 12, 13, 14) and continued to decline at all collection points past 30 days post-injection. Galactose levels generally show more correction than galactitol levels at all post-injection time points, with significance observed between M3 hGALT and M3 GFP/M3 UT galactose levels at 60 days post-injection.

In addition to liver metabolite levels, brain metabolite levels were also evaluated. Because liver GALT activity was detected in GALT assays discussed in Chapter 2 (Figure 2), brain metabolite quantification was conducted to discern if liver GALT restoration could affect metabolites in tissues outside of the liver. Brain GALT assays showed GALT activity in the brain was below detectable limits at each tissue collection time point (Figure 7). Although GALT activity was not assessed in other tissues that could express GALT such as muscle tissue, this observation supports that corrections in brain metabolite levels are likely the result of the increased liver GALT activity in M3 hGALT rats.

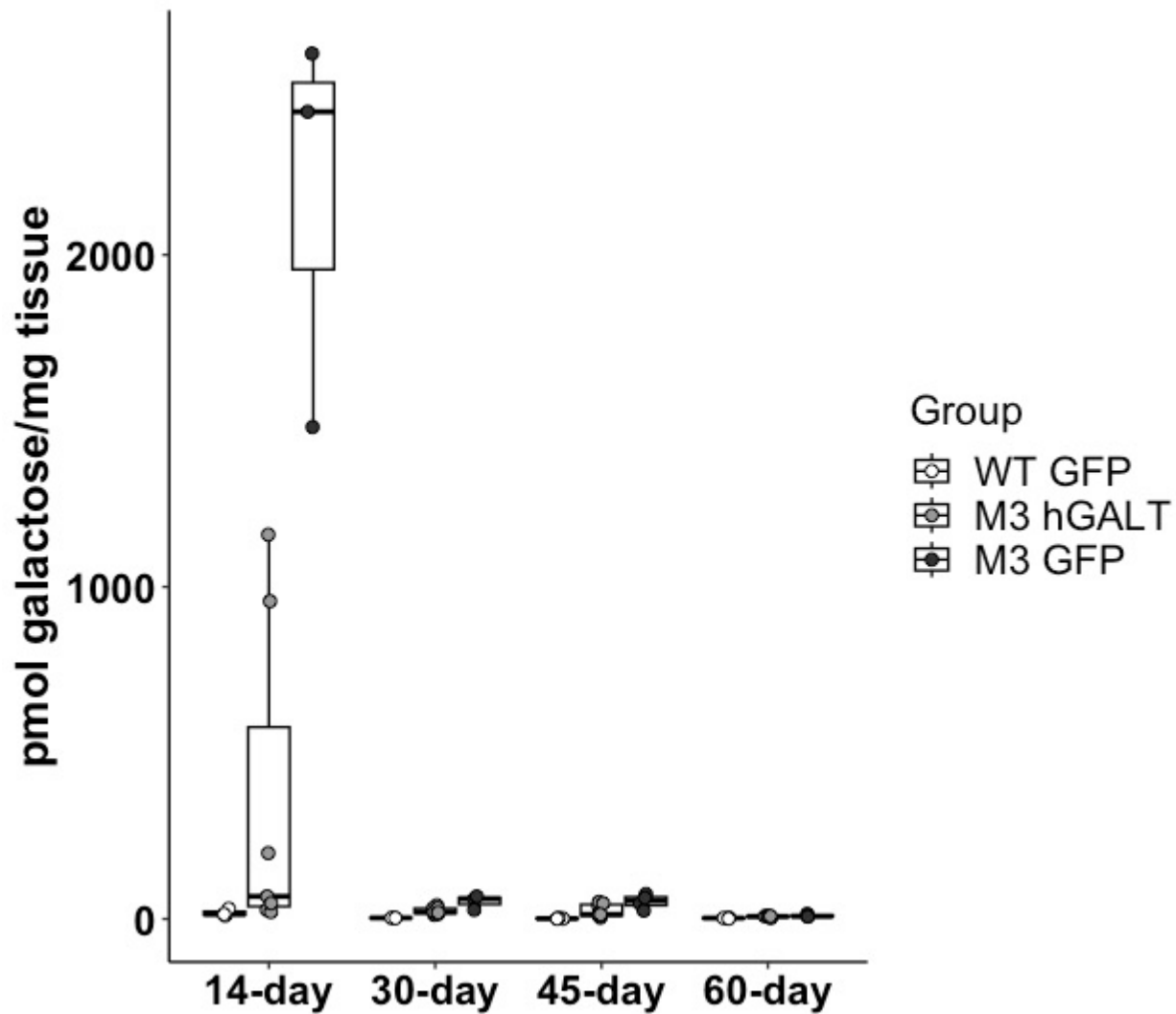


Figure 19. Brain galactose levels are shown for all post-injection tissue collection dates. At each collection point, data consist of 3 WT GFP, 6 – 7 M3 hGALT, and 3 – 4 M3 GFP samples.

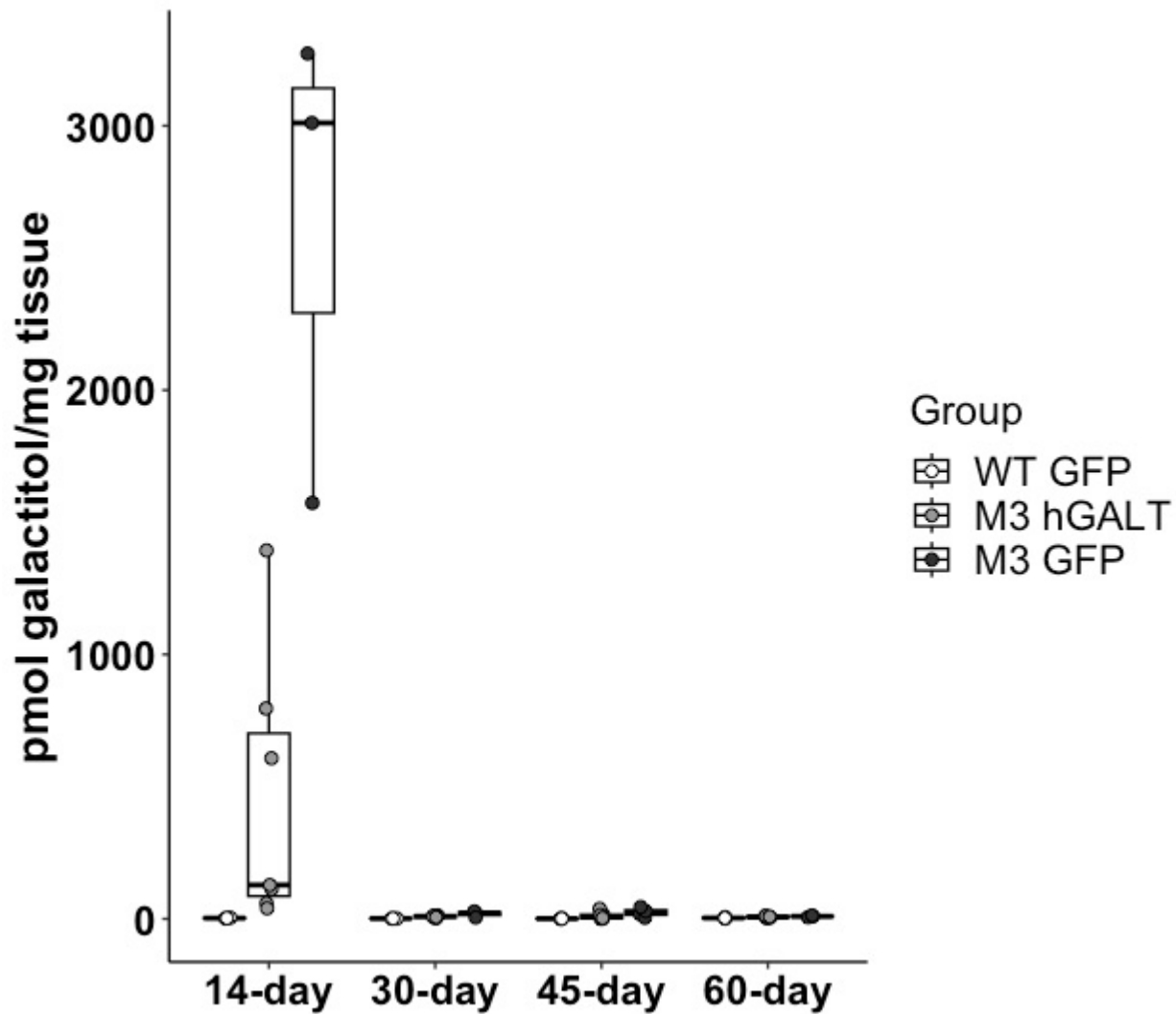


Figure 20. Brain galactitol levels are shown for all post-injection tissue collection dates. At each collection point, data consist of 3 WT GFP, 6 – 7 M3 hGALT, and 3 – 4 M3 GFP samples.

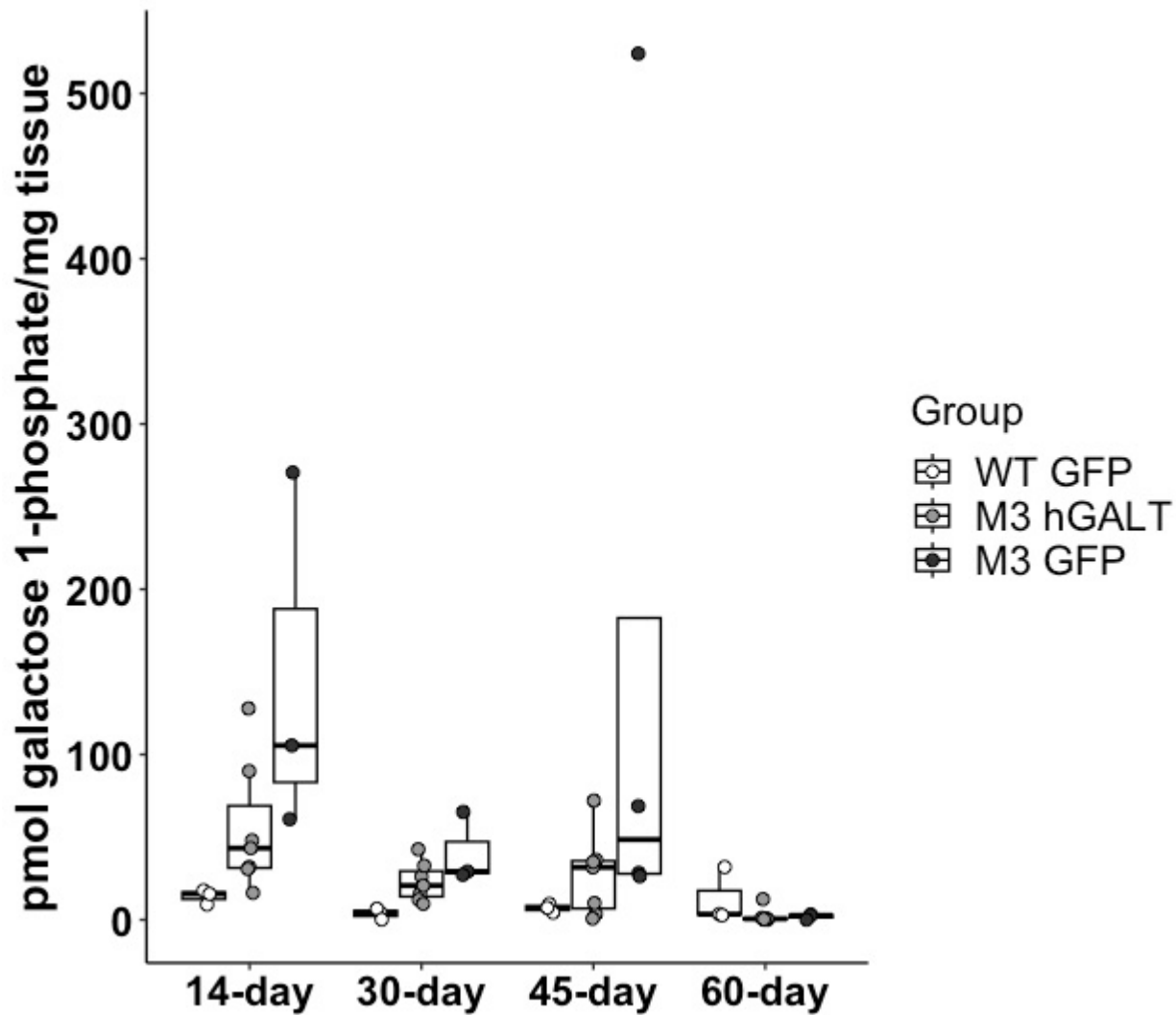


Figure 21. Brain Gal-1P levels are shown for all post-injection tissue collection dates. At each collection point, data consist of 3 WT GFP, 6 – 7 M3 hGALT, and 3 – 4 M3 GFP samples. Pairwise comparisons using Wilcoxon tests between M3 GFP and M3 hGALT: 14 days post-injection $p = 0.12$, 30 days post-injection $p = 0.18$, 45 days post-injection $p = 0.41$, and 60-days post-injection $p = 0.71$.

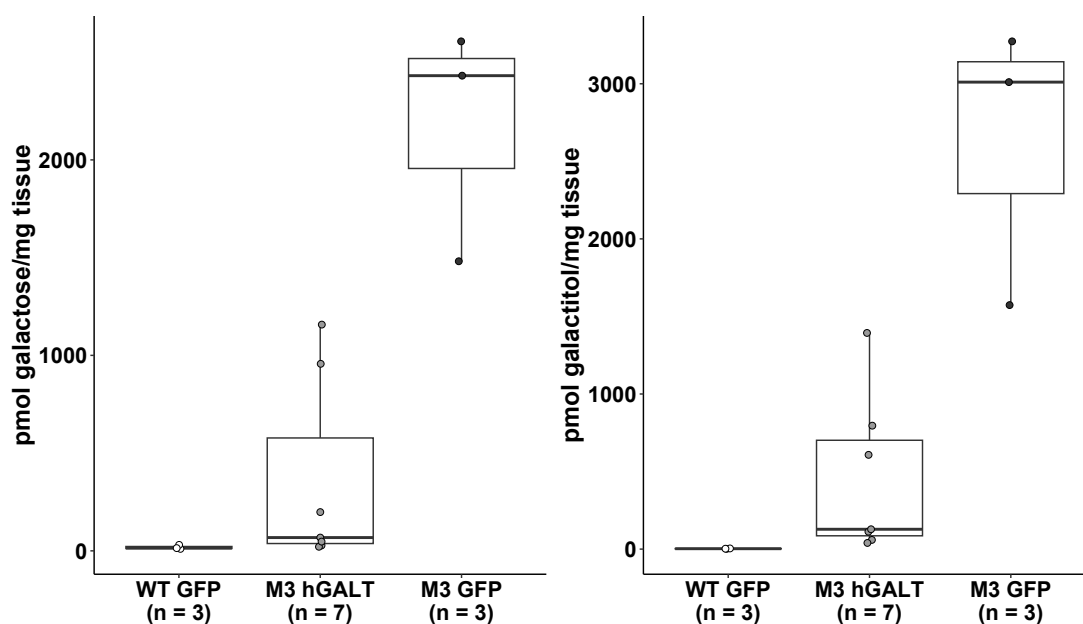


Figure 22. Brain galactose and galactitol levels are shown for brains collected 14 days post-injection. Pairwise comparisons using Wilcoxon tests between M3 GFP and M3 hGALT galactose yielded $p = 0.017^*$ and comparing galactitol $p = 0.017^*$.

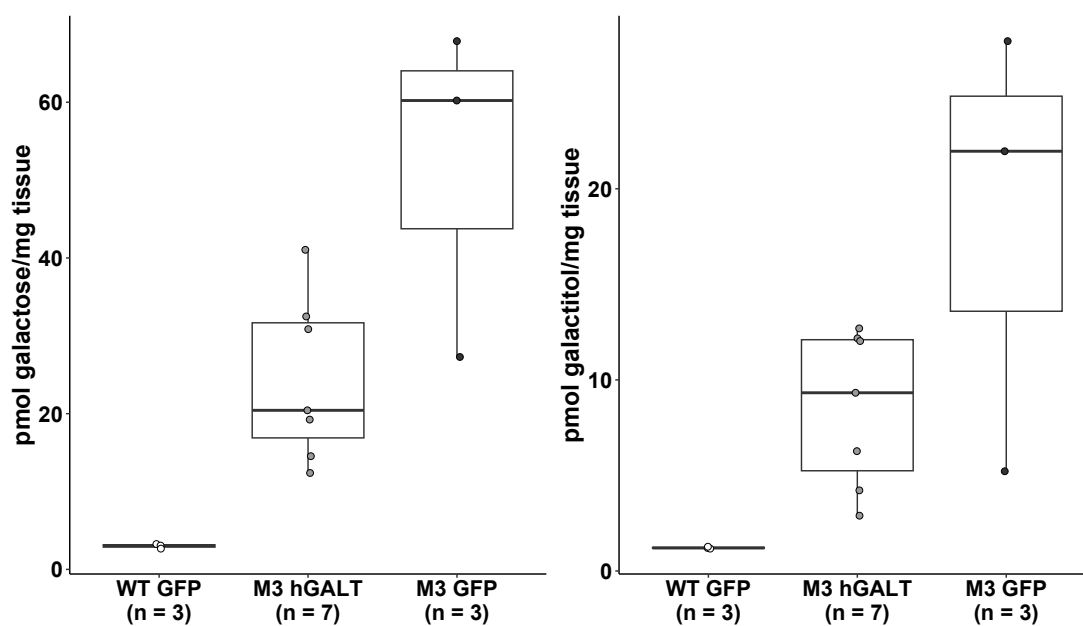


Figure 23. Brain galactose and galactitol levels are shown for brains collected 30 days post-injection. Pairwise comparisons using Wilcoxon tests between M3 GFP and M3 hGALT galactose yielded $p = 0.12$ and comparing galactitol $p = 0.27$.

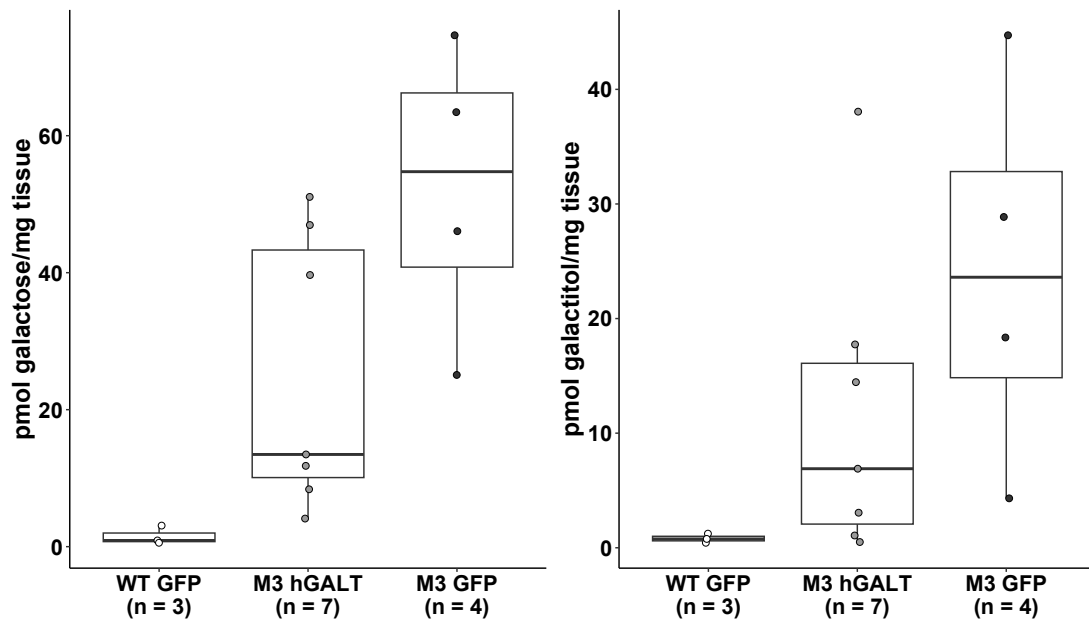


Figure 24. Brain galactose and galactitol levels are shown for brains collected 45 days post-injection. Pairwise comparisons using Wilcoxon tests between M3 GFP and M3 hGALT galactose yielded $p = 0.11$ and comparing galactitol $p = 0.16$.

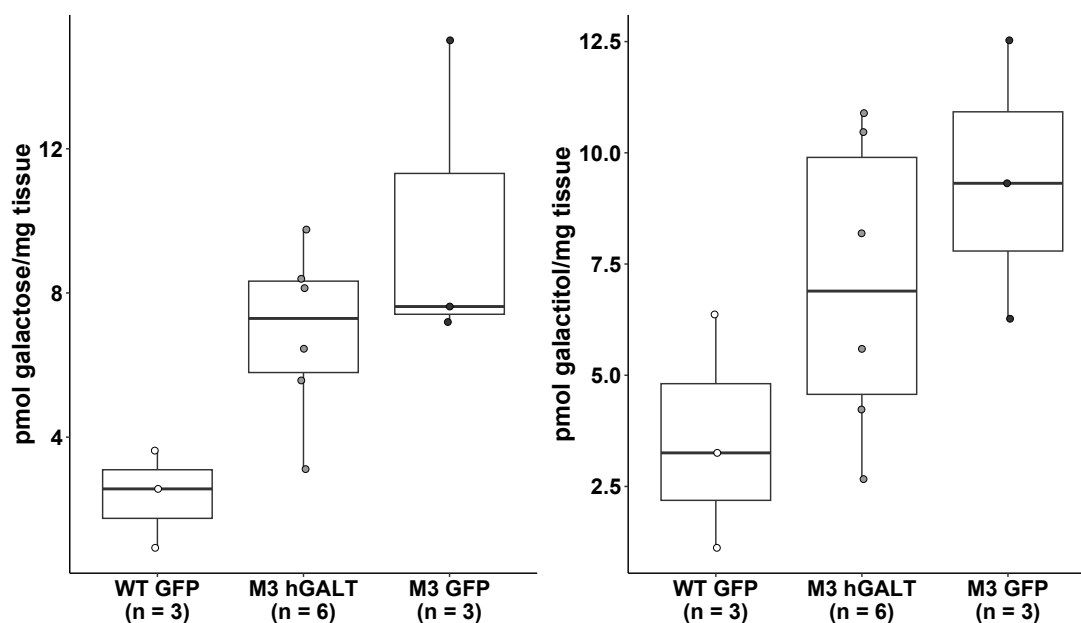


Figure 25. Brain galactose and galactitol levels are shown for brains collected 60 days post-injection. Pairwise comparisons using Wilcoxon tests between M3 GFP and M3 hGALT galactose yielded $p = 0.55$ and comparing galactitol $p = 0.38$.

Similar to the trends observed in the liver, metabolite levels in the brain show a general decrease in M3 hGALT rats compared to their M3 GFP counterparts, especially at 14 days post-injection. Both galactitol and galactose pairwise comparisons showed significance at 14 days post-injection (Figure 22), with no observance of significance at any other timepoint for all metabolites quantified.

Plasma metabolite levels were also assessed to reveal if liver GALT activity could offer some metabolite correction in blood components. Decreased galactose and galactitol levels in plasma may indicate that liver cells expressing the GALT transgene can reduce metabolite levels within the blood circulating throughout the organism. This would perhaps offer a degree metabolic rescue to tissues beyond the liver and broaden the impact of targeted liver GALT restoration on the organism as a whole.

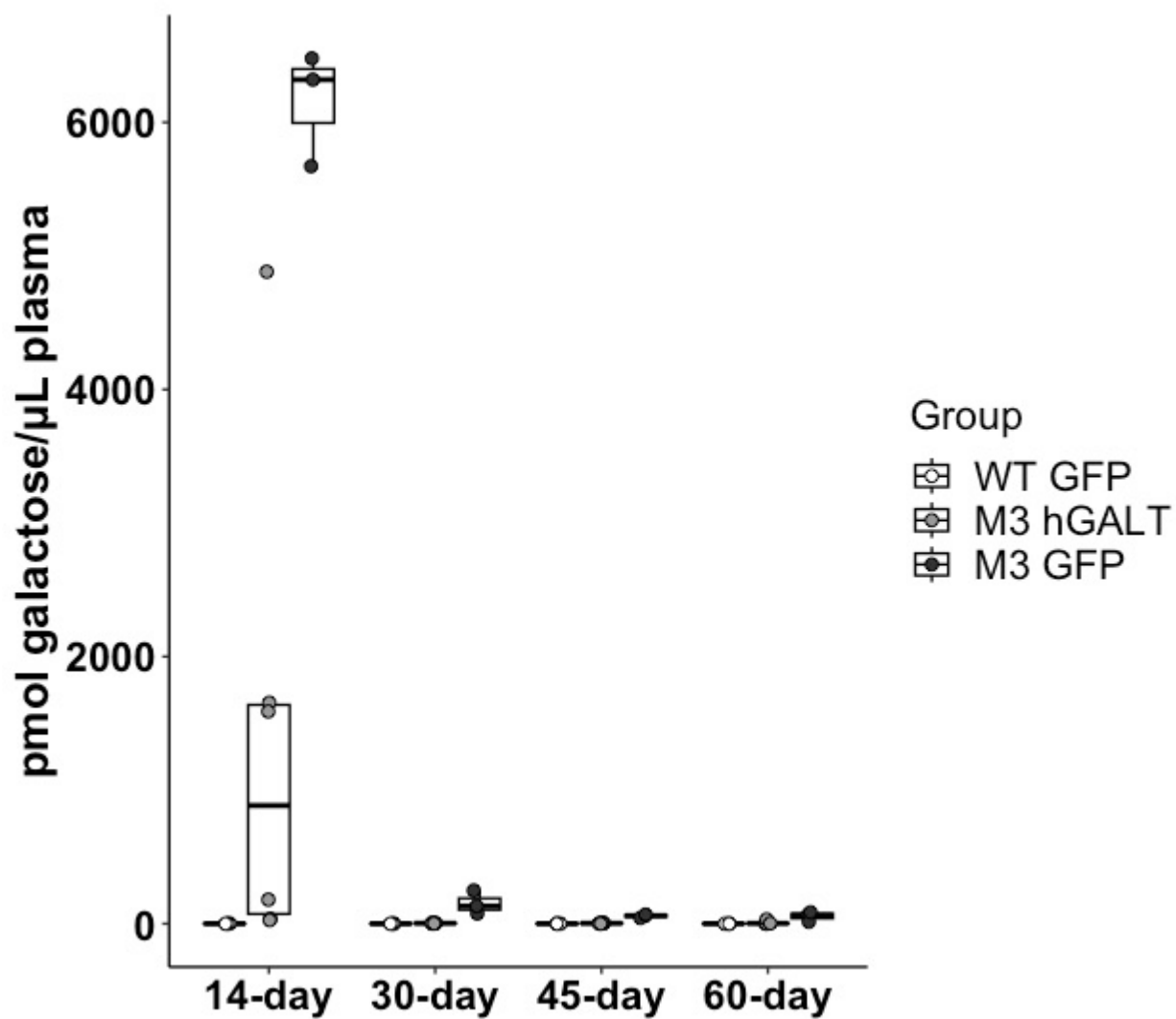


Figure 26. Plasma galactose levels are shown for all post-injection collection dates. All collection points consist of 3 WT GFP, 6 M3 hGALT, and 3 M3 GFP samples.

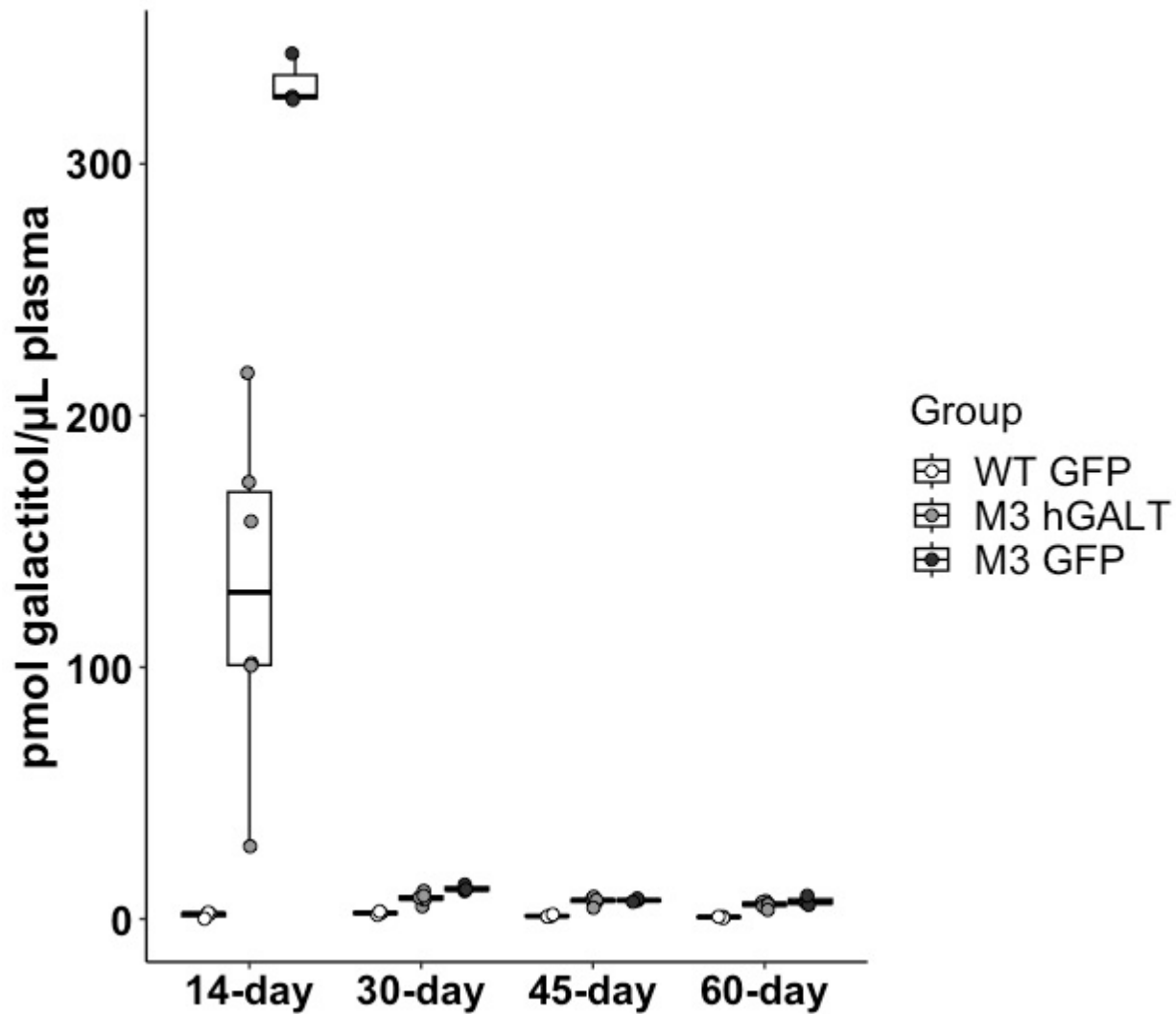


Figure 27. Plasma galactitol levels are shown for all post-injection collection dates. All collection points consist of 3 WT GFP, 6 M3 hGALT, and 3 M3 GFP samples.

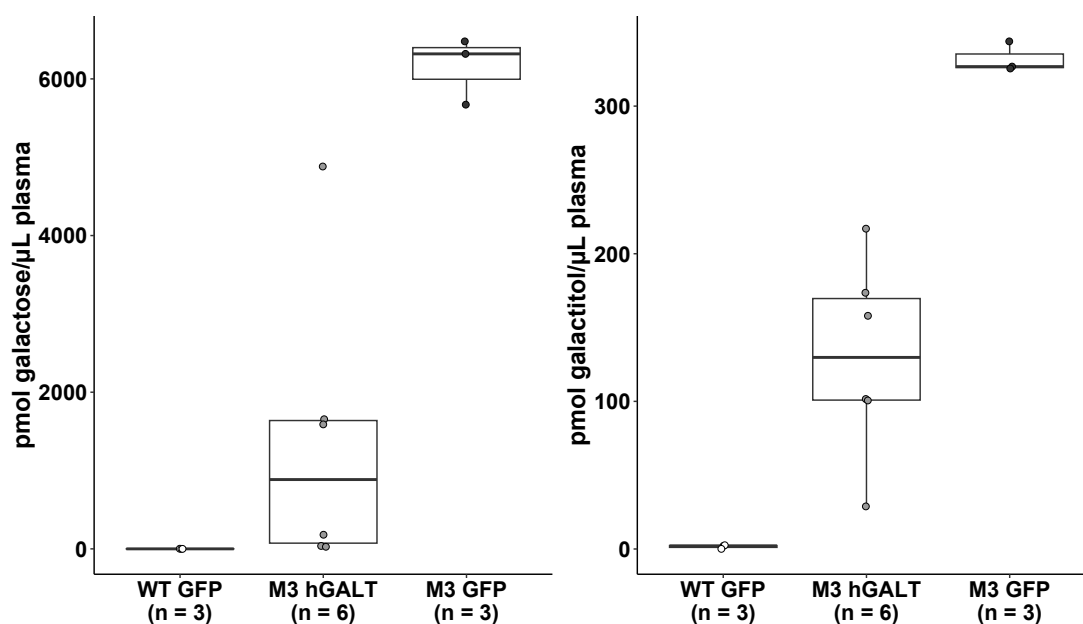


Figure 28. Plasma galactose and galactitol levels are shown for plasma collected 14 days post-injection. Pairwise comparisons using Wilcoxon tests between M3 GFP and M3 hGALT galactose yielded $p = 0.024^*$ and comparing galactitol $p = 0.024^*$.

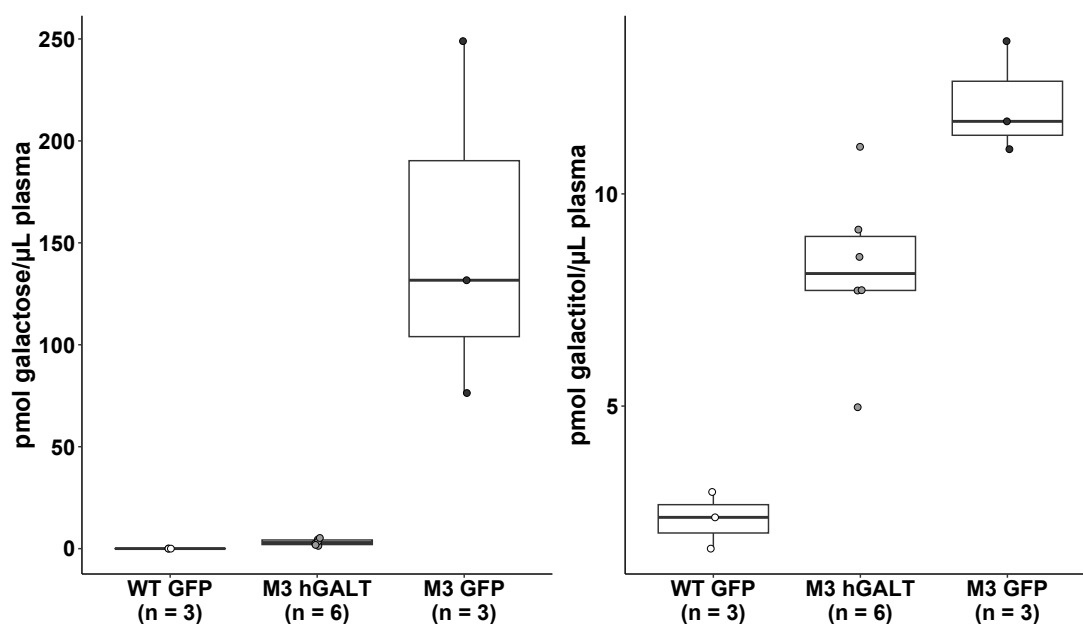


Figure 29. Plasma galactose and galactitol levels are shown for plasma collected 30 days post-injection. Pairwise comparisons using Wilcoxon tests between M3 GFP and M3 hGALT galactose yielded $p = 0.024^*$ and comparing galactitol $p = 0.048^*$.

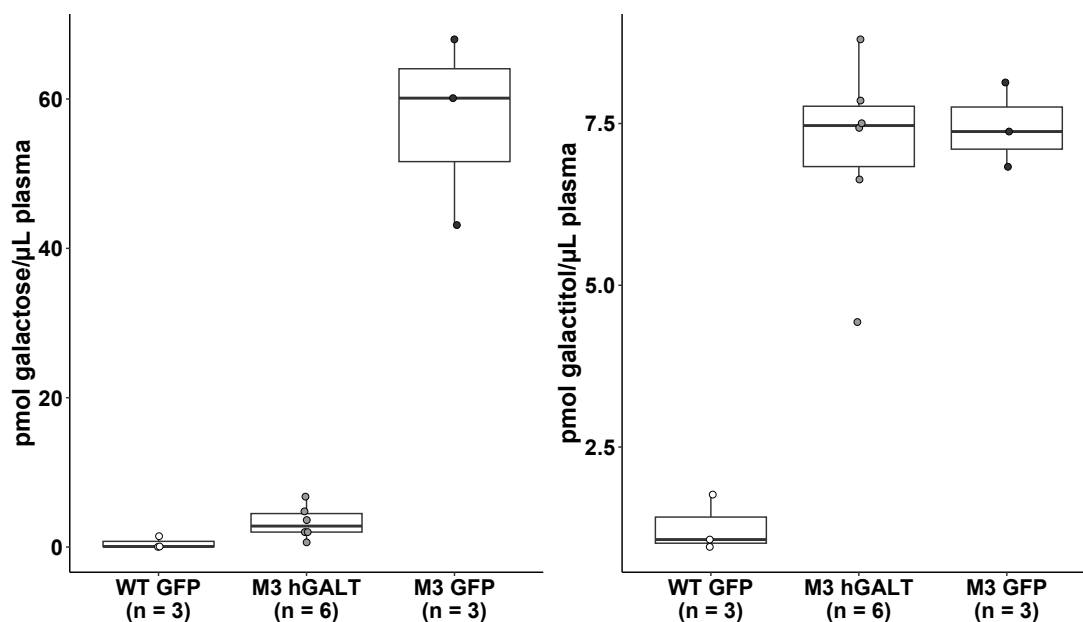


Figure 30. Plasma galactose and galactitol levels are shown for plasma collected 45 days post-injection. Pairwise comparisons using Wilcoxon tests between M3 GFP and M3 hGALT galactose yielded $p = 0.024^*$ and comparing galactitol $p = 1$.

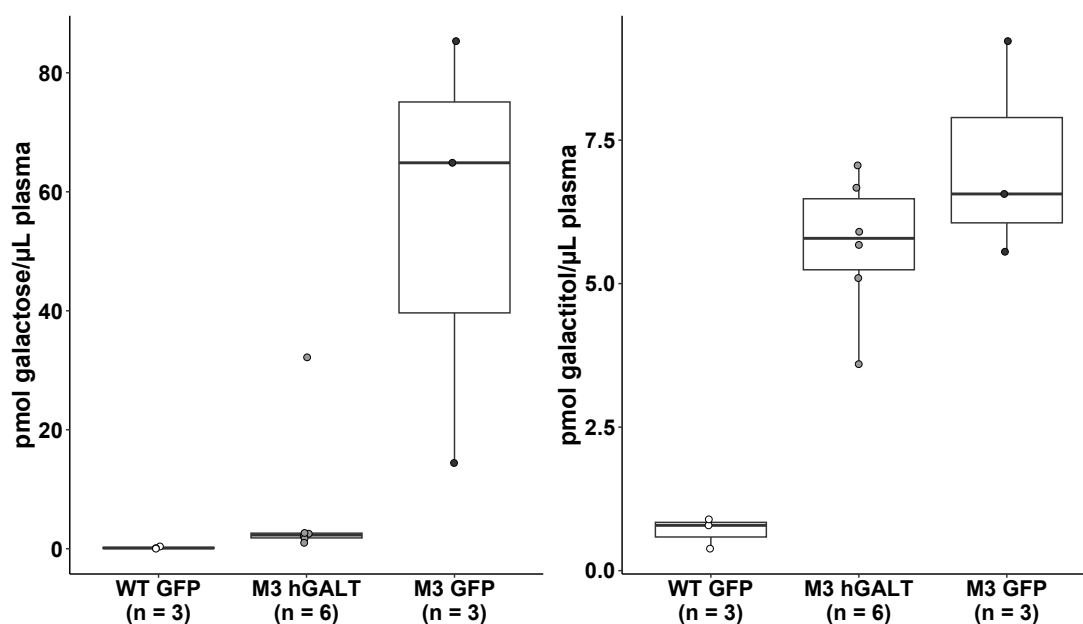


Figure 31. Plasma galactose and galactitol levels are shown for plasma collected 60 days post-injection. Pairwise comparisons using Wilcoxon tests between M3 GFP and M3 hGALT galactose yielded $p = 0.048^*$ and comparing galactitol $p = 0.55$.

Plasma galactose was generally decreased in the M3 hGALT group compared to the M3 GFP group, with significance observed at all time points. M3 GFP animals showed highest galactose levels at 14 days post-injection, and substantially decreased from 30 days post-injection onwards while still remaining elevated compared to WT GFP and M3 hGALT groups (Figure 26). Plasma galactitol levels showed some correction prior to 30 days post-injection in M3 hGALT rats, and gradually increased to levels comparable to the M3 GFP groups at later collection dates as supported by pairwise comparisons at 45 and 60 days-post injection (Figures 27, 30, 31).

Overall, metabolite analysis indicates metabolite level correction is most prominent during dates closer to injection administration. Although metabolite levels decrease across all groups as the age of the animal increases, metabolite quantification in the liver and brain shows a weak trend where M3 hGALT rats present with lower metabolite levels. In plasma, galactose appears to be corrected in M3 hGALT rats for a longer period of time when compared to galactitol correction. As with other tissues, the difference in galactose and galactitol levels in plasma samples is greatest at 14 days post-injection.

To assess if a relationship between metabolite levels and Liver GALT activity exists, metabolite levels at each post-injection tissue collection date were graphed against Liver GALT activity.

*Figures 32 – 41: animals collected 14 days post-injection are represented by circles, 30 days post-injection are represented by squares, 45 days post-injection are represented by diamonds, and 60 days post-injection are represented by triangles.

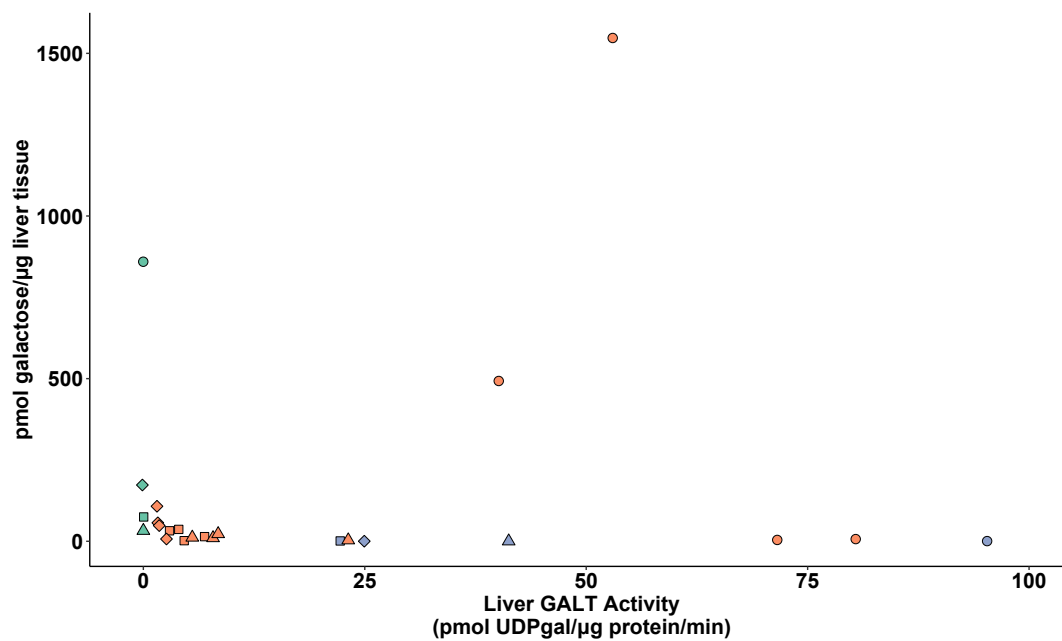


Figure 32. Relationship between liver galactose levels and liver GALT activity in WT GFP rats (blue), M3 hGALT rats (orange), and M3 GFP rats (green).

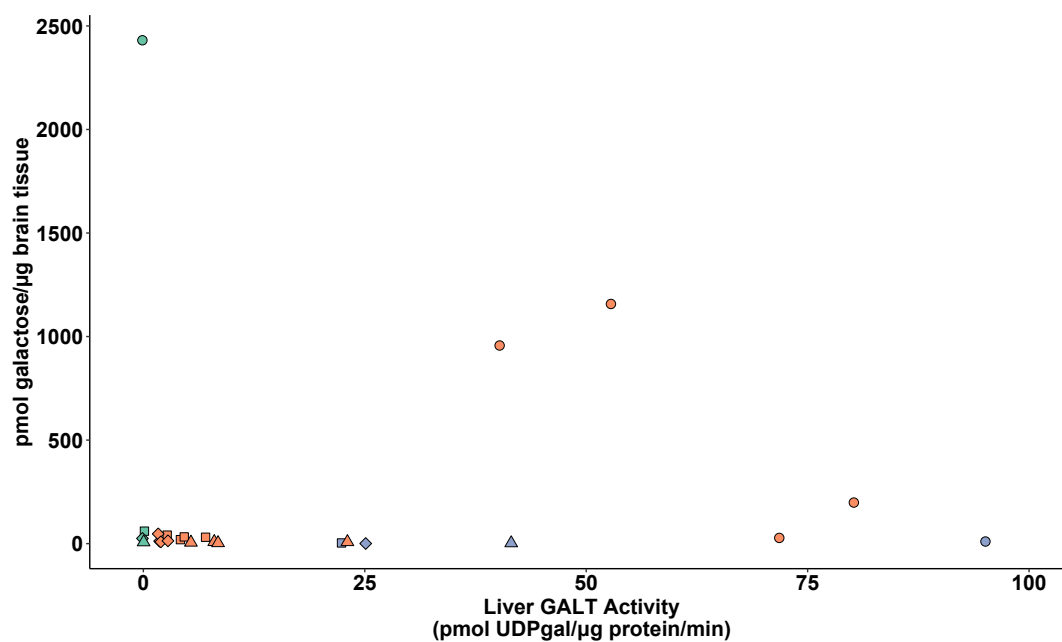


Figure 35. Relationship between brain galactose levels and liver GALT activity in WT GFP rats (blue), M3 hGALT rats (orange), and M3 GFP rats (green).

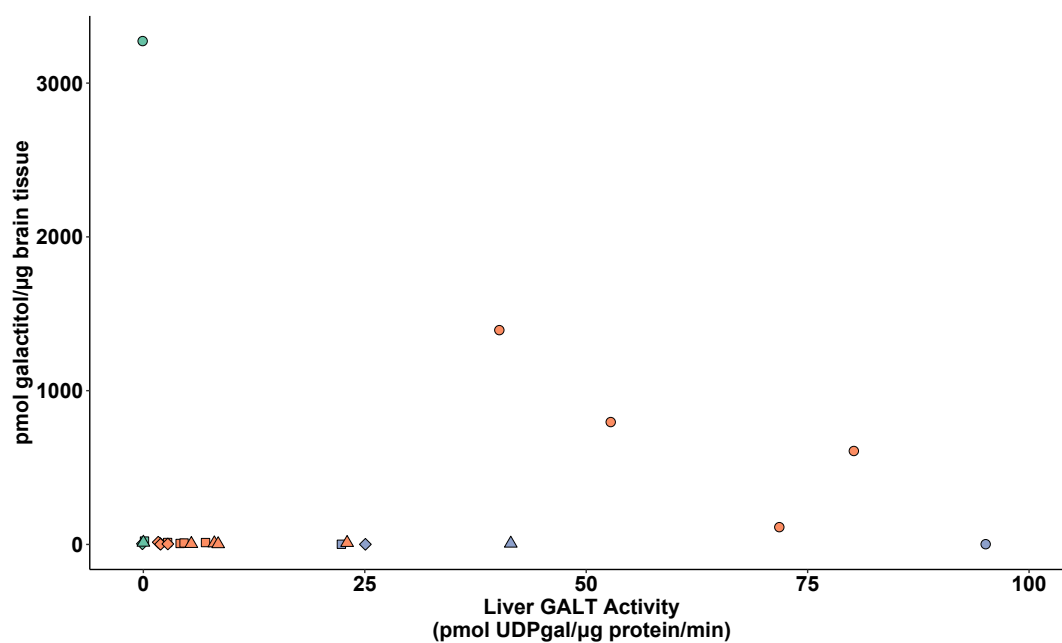


Figure 36. Relationship between brain galactitol levels and liver GALT activity in WT GFP rats (blue), M3 hGALT rats (orange), and M3 GFP rats (green).

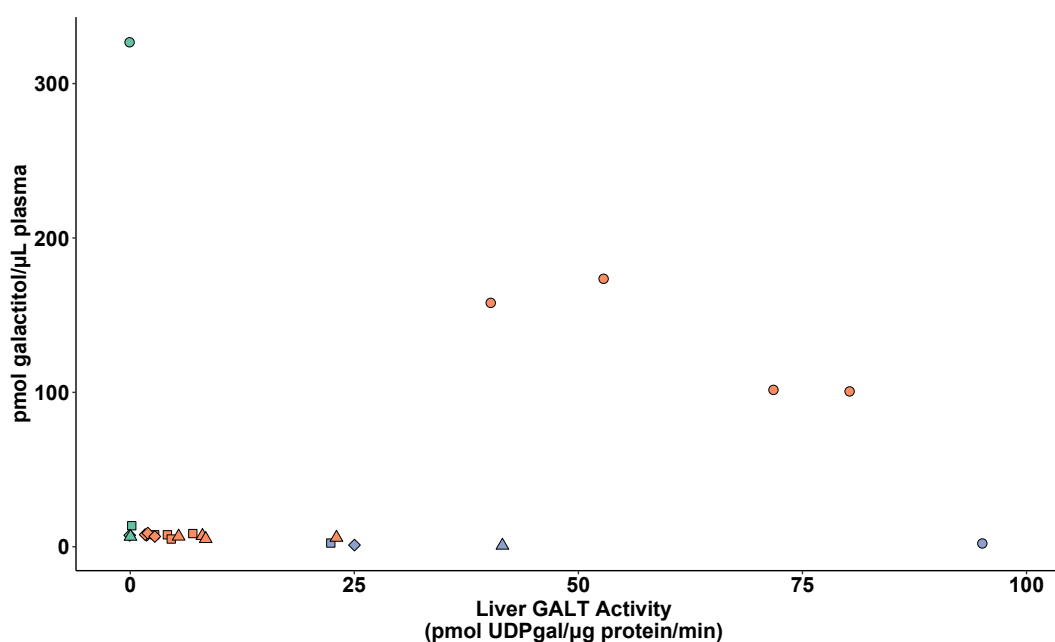


Figure 39. Relationship between plasma galactitol levels and liver GALT activity in WT GFP rats (blue), M3 hGALT rats (orange), and M3 GFP rats (green).

Discussion

Quantification of metabolites in liver, brain, and plasma displays some correction of metabolite levels in treated M3 hGALT rats. Across liver, brain, and plasma, galactose generally shows at least partial correction in M3 hGALT rats compared to M3 GFP rats (Figures 12, 13, 19, 20, 26, 27). Galactitol levels also show noticeable differences between M3 hGALT and M3 GFP rats during 14 days post-injection time points, but differences between these groups diminish as days post-injection increase. Gal-1P levels in the liver and brain suffer from high variance among samples. A weak trend may be present within the Gal-1P data, but possible outliers cannot be explained or eliminated with the current data (Figures 14, 21). In summary, some statistical differences do exist within the data, but these differences must be regarded with skepticism due to the small number of observations at each post-injection tissue collection date.

Examining the relationship shown between metabolite levels in tissues and plasma and liver GALT activity shows a weak correlation between higher liver GALT activity and diminished galactose, galactitol, and Gal-1P levels. As was expected, at all timepoints M3 GFP rats displayed GALT activity below detectable limits, while also presenting with exceptionally elevated metabolite levels. Likewise, WT GFP rats consistently showed high liver GALT activity along with little to no metabolite accumulation at any of the timepoints evaluated. The pattern of liver GALT activity decreasing in both WT GFP and M3 hGALT rats is clearly observed as the number of days since injection increases. With the exception of liver galactose and liver galactitol (Figures 32, 33), all 14 days post-injection M3 hGALT animals show lower galactose, galactitol, and Gal-1P levels than the M3 GFP animal collected at the same time point in each distribution. Most M3 hGALT rats also present with lower metabolite levels the higher their liver GALT activity is when compared to rats within their post-injection tissue collection date. This trend indicates that liver GALT restoration does indeed reduce metabolite levels not only in the liver, but also in the brain and plasma as well. Furthermore, the decrease in brain metabolites suggests that GALT restoration in the liver does offer some degree of protection to the brain even when brain GALT activity was not detected in GALT assays.

Previous studies of AAV gene therapy in GALT-null rat models have demonstrated that a small amount of GALT restoration in either the liver or brain significantly lowers galactose, galactitol, and Gal-1P in the liver and brain (13). However, there are two datapoints of concern within the distribution of metabolites versus liver GALT activity that do not follow the expected trend. 14 days post-injection animals with liver GALT activities at 40 and 53 pmol UDPgal/ μ g protein/min show higher than expected metabolite levels in distributions of liver galactose and liver galactitol (Figures 32, 33). These elevated levels are unlikely to be caused by biological

variation and could possibly be the product of a technical issue or error in executing the metabolite extraction protocol or GALT assay protocol. Until replicate samples from these rats are analyzed, these results cannot be designated as outliers.

CHAPTER 4 GENERAL DISCUSSION

Discussion

The current state of classic galactosemia research emphasizes a critical need for an effective therapeutic to improve the quality of life of patients living with CG. Of the strategies explored in research, gene therapy directly addresses the underlying cause of CG by restoring GALT function (1, 17). The objective of this investigation was to discern if the administration of AAV8-hAAT-HA-hGALT could yield liver-specific expression of GALT in a GALT-null rat model. As demonstrated through GALT assays performed on rats collected at 14, 30, 45, and 60 days post-injection, liver GALT activity was present in M3 hGALT rats. The GALT assays performed on brain samples revealed that GALT was not expressed in the brain within detectable limits, supporting the prediction that the use of an hAAT liver-specific promoter increases specificity of liver GALT restoration (9, 12). Furthermore, the results of GALT assays showed liver GALT activity decreases in rats as the days post-injection increase. This finding reflects current publications on AAV gene therapy, where transgene expression is reduced as a treated animal grows and develops (8, 18).

In addition to determining if liver-specific GALT restoration could be achieved by AAV8 mediated gene therapy, metabolite quantification of galactose, galactitol, and Gal-1P aimed to evaluate if liver GALT expression could provide metabolic rescue to both the liver as well as the brain and plasma in M3 hGALT rats. Overall, M3 hGALT rats generally showed reductions in metabolite levels, with the most prominent differences between M3 hGALT and M3 GFP metabolite levels observed at 14 days post-injection. Pairwise comparisons indicated some significant differences in the metabolite levels of M3 hGALT and M3 GFP animals, but the

reliability of these statistical tests was heavily limited by the small sample size available.

Analysis of the relationship between liver, brain, and plasma metabolite levels and liver GALT activity displayed a weak trend where increasing liver GALT activity correlated with decreased metabolite levels. Verification that brain GALT activity was below detectable limits at all timepoints in M3 hGALT rats suggests that differences in metabolite levels were the result of liver GALT restoration rather than combined GALT expression in the liver and brain. The beginnings of the trend observed in distributions of metabolite levels plotted against liver GALT activity indicated that the amount of GALT liver restoration achieved may be sufficient to provide a degree of metabolic rescue. If AAV8 mediated liver GALT restoration is pursued as a future therapeutic for CG, the most prominent differences in metabolite levels for animals collected 14 days post-injection are particularly encouraging. This pattern suggests AAV8 mediated liver GALT restoration may have an effect in early childhood prior to the onset of long-term health complications that frequently emerge by mid-childhood in human patients (1).

Limitations

The most prominent limitation of this investigation is the small sample size in both GALT assays and metabolite quantification. Although the animals analyzed represent only a fraction of the total animals available for this study, time limitations and sharing of equipment with other ongoing projects reduced the amount of data obtained for this project. GALT assays only consisted of a single WT GFP and M3 GFP animal at each of the four timepoints evaluated. The use of a single observation in each of these groups dramatically increases the influence of biological and technical variation on the GALT assay data. Additionally, statistical testing could not be performed on any of the GALT assay comparison groups due to the lack of multiple

observations in WT GFP and M3 GFP groups. Metabolite analysis also suffers from a lack of observations at each post-injection date. While preliminary pairwise comparisons were conducted on the data, these should be considered tentative results. Pairwise comparisons using the Wilcoxon rank sum tests were employed as a nonparametric test due to lacking sufficient observations to determine if the data were normally distributed; however, the statistical power of these comparisons is still hindered by the small sample size in metabolite data. Multiple post-injection timepoints also showed high variance in metabolite level calculations which further diminishes the reliability of calculated p -values.

Other limitations include the difficulty of performing tail-vein injections on rats at such a young age. All treatments were administered within 48 hours of birth (P2). The quality of the intravenous injection directly affects the amount of AAV8 vector that entered the circulatory system of a given rat, and consequently affects the transduction of the virus in the tissues of the animal. The quality of the virus injected may also affect the quantity of liver cells transduced following AAV8 administration. Both AAV8-hAAT-HA-hGALT and AAV8-hAAT-GFP viruses were produced in 2020. The supplier of the viruses states the shelf life of each virus is one year under proper storage conditions at -80° C. The majority of animals involved in this study were injected with the virus in 2021 with some animals receiving injections in 2022. Therefore, some animals received treatment after the latest administration date recommended by the producer. This may also affect the transduction of tissues in rats enrolled in this project after 2021.

Future Directions

Analysis of the data currently available in this investigation indicates AAV8 mediated GALT restoration was successful in the liver. Metabolite quantification also suggests a correlation between decreased metabolite levels and increased liver GALT activity. To improve statistical power of the liver GALT activity and metabolite level analyses, increasing the sample size in both areas would vastly improve the clarity of the present data. All samples used in this investigation represent only a portion of the total animals available for analysis. Within each post-injection collection date, between 4 to 7 additional observations could be added to WT GFP, M3 hGALT, and M3 GFP groups. Processing replicate samples from the same animal would also allow for the elimination of possible outliers within the study and establish more concrete conclusions on the study as a whole.

Aside from expanding sample sizes, additional GALT assays and metabolite quantification could provide a more holistic view of how AAV8 behaves within a GALT-null rat. Carrying out GALT assays on muscle tissue samples would determine if GALT activity is present within the tissue as was previously observed in other liver targeted AAV8 research (9). The use of the hAAT promoter should prevent detectable expression of GALT within muscle, which could be confirmed with muscle GALT assays. Rats collected at later post-injection dates also had blood samples taken from tail venipunctures. Examining the progression of blood metabolite levels in both RBCs and plasma would enable a longitudinal study of metabolite progression in the same animal.

Several other inquiries beyond GALT assays or metabolite quantification could be pursued to provide additional insight on the function of AAV8 mediated gene therapy in the GALT-null rat model. WT GFP and M3 GFP groups received an AAV8-hAAT-GFP injection,

containing green fluorescent protein for use in immunohistochemistry (IHC) quantification. Likewise, the AAV8-hAAT-HA-hGALT treatment contained an HA tag to allow binding of an anti-HA primary antibody for IHC. Liver, brain, muscle, heart, kidney, and ovary samples were collected from each rat and preserved as part of the tissue collection process. These samples could later be embedded, sectioned, and stained to quantify the fraction of IHC-stained cells. This procedure would reveal the presence or absence of AAV8 transduction in several of the tissues where AAV8 has previously infiltrated non-liver tissues in other animal studies (9). IHC would also allow for researchers to conclude if the fraction of stained cells decreases with days elapsed since post-injection and reveal if the transgene is being diluted as the liver develops in adolescent rats.

All rats were weighed daily up until weaning in addition to once every 7 days after weaning. Because prepubescent growth delay has previously been observed in both patient populations and GALT-null rat models (1), evaluating if growth delays are reduced in M3 hGALT rats could provide valuable information about the phenotypic efficacy of AAV8 mediated gene therapy. Eye slit lamp videos were also recorded and could provide the means to analyze the prevalence and severity of cataracts in treated and untreated GALT-null rats. Both of these avenues could improve understanding of phenotypic outcomes as a result of liver GALT restoration or metabolic rescue in GALT-null rats.

References

- (1) Fridovich-Keil, J. L.; Berry, G. T. Pathophysiology of Long-Term Complications in Classic Galactosemia: What We Do and Do Not Know. *Mol. Genet. Metab.* **2022**, *137* (1), 33–39. <https://doi.org/10.1016/j.ymgme.2022.07.005>.
- (2) Holden, H. M.; Rayment, I.; Thoden, J. B. Structure and Function of Enzymes of the Leloir Pathway for Galactose Metabolism *. *J. Biol. Chem.* **2003**, *278* (45), 43885–43888. <https://doi.org/10.1074/jbc.R300025200>.
- (3) Rasmussen, S. A.; Daenzer, J. M. I.; MacWilliams, J. A.; Head, S. T.; Williams, M. B.; Geurts, A. M.; Schroeder, J. P.; Weinshenker, D.; Fridovich-Keil, J. L. A Galactose-1-Phosphate Uridyltransferase-Null Rat Model of Classic Galactosemia Mimics Relevant Patient Outcomes and Reveals Tissue-Specific and Longitudinal Differences in Galactose Metabolism. *J. Inherit. Metab. Dis.* **2020**, *43* (3), 518–528. <https://doi.org/10.1002/jimd.12205>.
- (4) Berry, G. T. Galactosemia: When Is It a Newborn Screening Emergency? *Mol. Genet. Metab.* **2012**, *106* (1), 7–11. <https://doi.org/10.1016/j.ymgme.2012.03.007>.
- (5) *Galactosemia: MedlinePlus Genetics*. <https://medlineplus.gov/genetics/condition/galactosemia/> (accessed 2023-03-11).
- (6) Berry, G. T. Classic Galactosemia and Clinical Variant Galactosemia. In *GeneReviews®*; Adam, M. P., Mirzaa, G. M., Pagon, R. A., Wallace, S. E., Bean, L. J., Gripp, K. W., Amemiya, A., Eds.; University of Washington, Seattle: Seattle (WA), 1993.
- (7) Banford, S.; McCorvie, T. J.; Pey, A. L.; Timson, D. J. Galactosemia: Towards Pharmacological Chaperones. *J. Pers. Med.* **2021**, *11* (2), 106. <https://doi.org/10.3390/jpm11020106>.
- (8) Naso, M. F.; Tomkowicz, B.; Perry, W. L.; Strohl, W. R. Adeno-Associated Virus (AAV) as a Vector for Gene Therapy. *Biodrugs* **2017**, *31* (4), 317–334. <https://doi.org/10.1007/s40259-017-0234-5>.
- (9) Kattenhorn, L. M.; Tipper, C. H.; Stoica, L.; Geraghty, D. S.; Wright, T. L.; Clark, K. R.; Wadsworth, S. C. Adeno-Associated Virus Gene Therapy for Liver Disease. *Hum. Gene Ther.* **2016**, *27* (12), 947–961. <https://doi.org/10.1089/hum.2016.160>.
- (10) Nathwani, A. C.; Reiss, U. M.; Tuddenham, E. G. D.; Rosales, C.; Chowdary, P.; McIntosh, J.; Della Peruta, M.; Lheriteau, E.; Patel, N.; Raj, D.; Riddell, A.; Pie, J.; Rangarajan, S.; Bevan, D.; Recht, M.; Shen, Y.-M.; Halka, K. G.; Basner-Tschakarjan, E.; Mingozzi, F.; High, K. A.; Allay, J.; Kay, M. A.; Ng, C. Y. C.; Zhou, J.; Cancio, M.; Morton, C. L.; Gray, J. T.; Srivastava, D.; Nienhuis, A. W.; Davidoff, A. M. Long-Term Safety and Efficacy of Factor IX Gene Therapy in Hemophilia B. *N. Engl. J. Med.* **2014**, *371* (21), 1994–2004. <https://doi.org/10.1056/NEJMoa1407309>.

- (11) Sands, M. S. AAV-Mediated Liver-Directed Gene Therapy. In *Adeno-Associated Virus: Methods and Protocols*; Snyder, R. O., Moullier, P., Eds.; Methods in Molecular Biology; Humana Press: Totowa, NJ, 2011; pp 141–157. https://doi.org/10.1007/978-1-61779-370-7_6.
- (12) Grimstein, C.; Choi, Y.-K.; Wasserfall, C. H.; Satoh, M.; Atkinson, M. A.; Brantly, M. L.; Campbell-Thompson, M.; Song, S. Alpha-1 Antitrypsin Protein and Gene Therapies Decrease Autoimmunity and Delay Arthritis Development in Mouse Model. *J. Transl. Med.* **2011**, *9*, 21. <https://doi.org/10.1186/1479-5876-9-21>.
- (13) Daenzer, J. M. I.; Rasmussen, S. A.; Patel, S.; McKenna, J.; Fridovich-Keil, J. L. Neonatal GALT Gene Replacement Offers Metabolic and Phenotypic Correction through Early Adulthood in a Rat Model of Classic Galactosemia. *J. Inherit. Metab. Dis.* **2022**, *45* (2), 203–214. <https://doi.org/10.1002/jimd.12471>.
- (14) Sengupta, P. The Laboratory Rat: Relating Its Age With Human's. *Int. J. Prev. Med.* **2013**, *4* (6), 624–630.
- (15) Rostami Dovom, M.; Noroozadeh, M.; Mosaffa, N.; Zadeh–Vakili, A.; Piryaei, A.; Ramezani Tehrani, F. Induced Premature Ovarian Insufficiency by Using D Galactose and Its Effects on Reproductive Profiles in Small Laboratory Animals: A Systematic Review. *J. Ovarian Res.* **2019**, *12* (1), 96. <https://doi.org/10.1186/s13048-019-0565-6>.
- (16) Coelho, A. I.; Rubio-Gozalbo, M. E.; Vicente, J. B.; Rivera, I. Sweet and Sour: An Update on Classic Galactosemia. *J. Inherit. Metab. Dis.* **2017**, *40* (3), 325–342. <https://doi.org/10.1007/s10545-017-0029-3>.
- (17) Delnoy, B.; Coelho, A. I.; Rubio-Gozalbo, M. E. Current and Future Treatments for Classic Galactosemia. *J. Pers. Med.* **2021**, *11* (2), 75. <https://doi.org/10.3390/jpm11020075>.
- (18) Penaud-Budloo, M.; Le Guiner, C.; Nowrouzi, A.; Toromanoff, A.; Chérel, Y.; Chenuaud, P.; Schmidt, M.; von Kalle, C.; Rolling, F.; Moullier, P.; Snyder, R. O. Adeno-Associated Virus Vector Genomes Persist as Episomal Chromatin in Primate Muscle. *J. Virol.* **2008**, *82* (16), 7875–7885. <https://doi.org/10.1128/JVI.00649-08>.